

Department of Precision and Microsystems Engineering

Towards A Robust Component Transfer Path Analysis Method

Eric Antonie Pasma

Report no : EM 2014.026
Coach : Ir. M. Van der Seijs
Professor : Prof.dr.ir F. Van Keulen
Specialisation : EM
Type of report : MSc. thesis
Date : 16 October 2014

Towards A Robust Component Transfer Path Analysis Method

Application and Validation in Automotive Research

MASTER OF SCIENCE THESIS

For the degree of Master of Science in Engineering Dynamics
at Delft University of Technology

AUTHOR

E.A. Pasma

COMMITTEE

Ir. M. Van der Seijs

Ir. M. Fenzl

Dr.ir. D. De Klerk

Prof.dr.ir. F. Van Keulen

October 24, 2014

Faculty of Mechanical, Maritime and Materials Engineering (3mE)
Delft University of Technology



Copyright © Precision and Microsystems Engineering (PME)
All rights reserved.

Abstract

A robust Transfer Path Analysis (TPA) procedure is presented to predict the transmitted vibrations of a steering gear in BMW vehicles in a multi-kHz range. The internal excitation forces are characterised as a set of equivalent forces on the interface of the active component. These equivalent forces are determined from force and acceleration measurements at the interface of the active component and a test bench. The response of the total system is calculated with the dynamic properties at the component interface onwards to a point of interest in the vehicle. Two equivalent force determination schemes are applied on two test benches with different dynamic properties. The first method relies on direct interface force measurements, whereas the second procedure is based on a matrix inverse procedure on the assembly of the steering gear and the test bench. It is shown that these equivalent forces are indeed a property of the active component only.

All methods use the virtual point transformation to build a nodal description on interfaces of the structures. This is a crucial step in Dynamic Substructuring (DS) for the connectivity between the substructures. The projection of measured Frequency Response Functions (FRFs) on local rigid interface displacement modes in a user-specified virtual point, which allow to determine rotational degrees of freedom, that are in practice unmeasurable, yet crucial for the connectivity. Pre-analysis on the transformation to interface degrees of freedom and a sufficient over-determination, enhance noise suppression and mode observability. This method is validated by means of a benchmark of three identical vehicles of which the virtual point dynamics are determined on the interface of the steering gear and the vehicle.

For a robust prediction and to get grip on the uncertainties in the analyses, all steps are evaluated separately and qualified with performance indicators.

Acknowledgements

After the completion of my MSc. thesis I gave myself the time to reflect on a special period in my life. My graduation project has been much more than just the final project to finish my studies at Delft University of Technology. The opportunity to perform a research project at the research and development facilities of BMW in Munich has been truly exciting. Besides all scientific and practical challenges during the project, I have developed myself on a personal level and enjoyed life in Munich and its surroundings.

First of all, I would like to thank Maarten van der Seijs for asking me to take part of his research project. Due to his inspiration and energy, it was a pleasure to work on my thesis. It was a pleasure to work together and I have enjoyed our endless discussions.

I appreciate the support of Dennis de Klerk during the project. During the few meetings we have had at BMW, I am inspired by his enthusiasm and positive energy.

Furthermore, I would like to express my gratitude to Matthias Fenzl. He has been very supportive and it was a pleasure to work together. He has been important to get around in the company. Through him, I got into contact with various people and departments crucial for the success of the project.

I would like to thank my former colleagues of the department EG-431, *Mechatronik Gesamtfahrzeug* at BMW for their cooperation and creating a pleasant working atmosphere.

Last but not least, I want to express my appreciation to my family, friends and all people I have met during my time in Munich. Everyone has been truly supportive and all encouragements inspired me to give my best and enjoy my time in Germany.

Leeuwarden,
October 2014

Eric Pasma

Table of Contents

Abstract	i
Acknowledgements	iii
Introduction	vii
Research Context	vii
Thesis Assignment	viii
Thesis Outline	ix
Nomenclature	xi
List of Acronyms	xi
I General Theory	1
1 General introduction to Transfer Path Analysis	3
1.1 Classical TPA methods	4
1.1.1 Limitations of classical TPA methods	6
1.2 Component-based TPA methods	7
1.2.1 The equivalent source problem	9
1.2.2 Equivalent response at passive side	9
1.2.3 Equivalent forces from test bench measurements	10
1.2.4 General remarks on equivalent force procedures	12
1.3 Summary	13

2	Obtaining Dynamic models from measurements	15
2.1	Theory on Virtual Point Transformation	16
2.1.1	A note on the virtual point transformation	17
2.1.2	Monitoring the quality	18
2.1.3	Practical considerations	19
2.2	Example	21
2.3	Summary	25
II	Practice	27
3	Industrial Test Case	29
3.1	System description	30
3.2	Test Benches	31
3.3	Operational Conditions	32
3.4	Operational rack bar forces	33
3.5	Validation strategy	33
3.6	Application	35
3.6.1	Validation Measurement	36
3.6.2	Total vehicle FRF Measurement	36
3.6.3	Test bench TB1 + steering gear	37
3.6.4	Test bench TB2 + steering gear	38
3.6.5	Operational Measurements	41
3.6.6	Equivalent forces	44
3.6.7	Noise prediction	47
3.7	Summary	48
III	Conclusions and Recommendations	51
A	Frequency Response Function	57
B	Dynamic Substructuring	59
C	Experimental Modal Analysis	61
D	Experimental FRF Determination	65
D.1	Practical Considerations	67
E	Complex Mode Indicator Function	71
F	Test Benches	73
G	Measurement Equipment	79
H	Matlab Toolbox	81

Introduction

The word 'auto-mobile' is a compound word, which literally means *self moving*. This word originates from the Greek *αυτός* (self) and the Latin *movere* (to move). Self - or personal - reflects nicely the activities of the *Bayerische Motoren Werke Aktiengesellschaft* or **BMW AG**, which are focussed on the development of premium products and premium services for individual mobility [19].

Nowadays, the market demands a lot from premium cars: driving performance, aesthetics, safety, comfort, etcetera. Besides these demands, society wishes for the reduction of the environmental impact of companies. In the automotive industry this is reflected by the trend towards lightweight designs, the development of hybrid/electric powertrain concepts and the replacement of hydraulic-assisted systems by mechatronic parts.

The driving experience is highly influenced by the acoustic experience in the interior of the car. The trends towards quieter and electrified vehicles make that the traditional wind, tire and engine noise become less dominant while the electric powertrain and mechatronic components become more prominent noise sources, especially at lower speeds and in a higher frequency bandwidth. Therefore, enhanced tools to analyse and predict noise and vibration problems in cars are highly desired.

The increasing complexity of cars make that numerous components are developed by specialised external companies in collaboration with the car manufacturer. To stay ahead of competition and to build *premium* cars, BMW has to make use of detailed specifications and strict (noise-)targets for the components towards the supplier to optimise the car as a whole. Moreover, due to the increasingly shorter car development cycles or *time-to-market*, there is need for an early identification of noise and vibration problems. Therefore, accurate models of the dynamic behaviour of complex structures are required based on the knowledge of the dynamic properties of its (sub)components to set targets for suppliers.

Research Context

These challenges in recent vehicle development have led to the project *Ableitung Komponentenziele Mechatronik* at the BMW Research and Development Centre in Munich, Germany. This project is headed by PhD candidate Ir. M.V. van der Seijs of Delft University of Technology. The main goal of this project is to develop methods for the accurate prediction of the

noise and vibration propagation of the internal excitations of an operating steering gear to the acoustic pressure at the driver's ear in the frequency range of 50 up to several kHz.

Transfer Path Analysis

Transfer Path Analysis (TPA) is an experimentally based method to analyse the propagation of structure-borne noise and vibration of an active component to a point of interest on the receiving structure. This method describes the vibration or interior sound pressure levels at a point of interest as the sum of all transfer path contributions of the individual systems [27, 31]. The measured Frequency Response Functions (FRFs) of the transfer paths are multiplied with the operational excitation spectra of the active component which are estimated e.g. for the total assembly. In these *classical TPA* methods, the operational excitation spectra are dependent on the configuration in the total vehicle. This disadvantage limits the method to identifying dominant transfer paths and make the methods not suitable for component-wise optimisation.

Much effort has been put in obtaining operational excitations as a property of the active component only. These methods are classified as *component TPA* methods. In these methods the operational excitations can be characterised as *equivalent forces* on a test bench. The equivalent forces are multiplied with the total system FRFs from the active components interface to response nodes of interest. This leads to a prediction with physically correct transfer paths. These total system FRFs can be obtained by e.g. experimental Dynamic Substructuring (DS) [24].

Measuring the equivalent forces of the active component against a fully rigid test bench, one obtains *blocked-forces*. As a test bench will not be rigid in the considered frequency range, one can compensate for test bench flexibility to obtain the equivalent forces [9, 23].

Rather than directly measured blocked forces, one can alternatively obtain equivalent forces by methods that rely on interface *motion* in a matrix-inverse procedure on the test bench with the active component mounted [14, 28, 29].

Thesis Assignment

While various component TPA methods conceptually lead to the same physically correct prediction, practical issues withhold successful noise prediction in a multi-kHz bandwidth [9]. Therefore, the equivalent interface forces will be determined using multiple approaches with an in-depth discussion on all steps of the analysis. As the dynamic properties of the test bench influence the determination of the equivalent forces, it will be investigated what is practically required for a test bench. Furthermore, practical challenges regarding experimental FRF-based modelling of interfaces [36] will be attempted to solve and again, all steps will be closely monitored.

To perform the complete component TPA robustly, quality indicators are formulated in all steps to enhance the quality of the analysis. All these topics can be integrated in the general thesis assignment:

"Develop a robust strategy to perform component Transfer Path Analysis in a multi-kHz range on complex systems using experimental Dynamic Substructuring techniques"

To fulfil the requirements of this assignment and ultimately perform robust component TPA, the presented methodology will be applied on the steering gear. Two equivalent force determination schemes will be applied on two different test benches to qualify the strategy.

Thesis Outline

This thesis consists of three parts. The first part the general theory on TPA is presented. This part is partly based on the paper [35]. The second chapter addresses the modelling of structures with measurements, which is validated by a benchmark example. In the second part the theory presented in part I is applied to the steering gear. Conclusions and recommendations are given in part III. In the appendices some necessary background information is written which are less critical for understanding the analysis approach, but perhaps crucial for conducting the separate steps. Where is referred to the appendices, the reader is encouraged to read those as well.

Part I: Theory

- Chapter 1 covers the concepts of classical TPA to show its limitations. Hereafter, various component-based TPA methods are derived, based on the dynamics of the subsystems.
- Chapter 2 addresses the virtual point transformation which is a key concept in the thesis for the connectivity of the structures. Multiple quality indicators are introduced to get a grip on the transformation. The theory will be validated with a practical example.

Part II: Practice

- The theory described in the previous chapters is applied to the steering gear vibration transmission. The structures are described and the validation strategy outlined. Lots of attention is paid to the qualification of the two test benches. Hereafter, all steps in the analysis are discussed.

Part III: Conclusions and Recommendations

- In the third and final part, conclusions and recommendations for future work are listed.

Appendices

- A The derivation of Frequency Response Functions (FRFs) from the Equations of Motion;
- B The derivation of the Lagrange Multiplier Frequency Based Substructuring (LM-FBS) algorithm;
- C Derivation of the pole/residue model and a modal parameter identification method;
- D Theoretical and practical aspects of experimental FRF determination;
- E The Complex Mode Indicator Function (CMIF) explained;
- F Detailed description of the test benches;
- G Listed details on the measurement equipment;
- H A short description of the MATLABtools used during the project.

Nomenclature

List of Acronyms

BMW AG	Bayerische Motoren Werke Aktien Gesellschaft
CMIF	Complex Mode Indicator Function
DoFs	Degrees of Freedom
DS	Dynamic Substructuring
EoM	Equations of Motion
EPS	Electric Power Steering
FEM	Finite Element Model
FBS	Frequency Based Substructuring
FIZ	Forschungs- und Innovationzentrum
FRFs	Frequency Response Functions
IDM	Interface Displacement Mode
LM-FBS	Lagrange Multiplier Frequency Based Substructuring
MAC	Modal Assurance Criterion
NVH	Noise, Vibration & Harshness
TB	Test Bench
TPA	Transfer Path Analysis
VP	Virtual Point

Part I

General Theory

Chapter 1

General introduction to Transfer Path Analysis

Noise and vibration paths are investigated by the use of Transfer Path Analysis (TPA) to analyse and understand the contribution of components and its transfer paths to the global noise and vibration levels in the car. All concepts are illustrated by the coupled structure AB , consisting out of two substructures, a source component A and a receiving structure B . The active subsystem A contains the excitation source in node 1. The receiving substructure comprises the responses of interest at node 3, which can be either structural responses or acoustic pressures in case of interior noise in a car or a combination of the two. A typical Transfer Path Analysis (TPA) problem is illustrated in figure 1.1. Generally, one can speak of two types of source systems

1. *Subsystems with fixed interfaces.* Consider the excitations generated by the spindle and belts inside the steering gear of a car. To analyse how these vibrations propagate through the car to a point of interest, the connection points of the system need to be properly fixed to operate normally. Therefore, this vibration source has to be characterised as interface forces at the connection points.
2. *Subsystems with free interfaces.* Consider the vibrations of a factory floor on which a high-precision machine is installed. To meet precision targets of the product machined by the company, the transferred vibrations from the floor (source) to a point of interest on the machine (receiver) have to be analysed. It is not practical to characterise the interface forces of a rigidly constrained floor, but the vibration source is preferably characterised by acceleration levels of the free-vibrating floor.

The two substructures are coupled at the interface Degrees of Freedom (DoFs) at node 2. For the sake of simplicity, it is assumed that the numbering on both sides of the interface of the substructures A and B is the same. The structural dynamics of both domains s can be described in the frequency domain by either the dynamic stiffness/impedance $\mathbf{Z}^s(\omega)$ or the receptance/admittance $\mathbf{Y}^s(\omega)$. The displacements of a substructure are denoted with the set

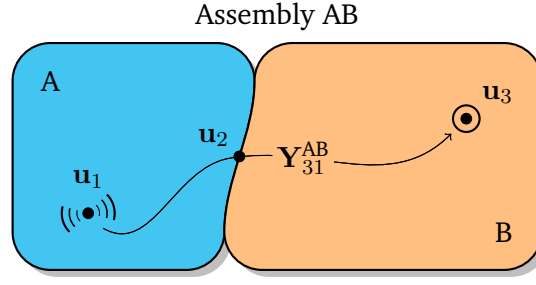


Figure 1.1: The transfer path problem

$u^s(\omega)$, the vectors $f(\omega)$ and λ indicate the applied forces and the interface forces respectively, as shown in figure 1.1.¹ As in this thesis the dynamic properties of the substructures are determined by the use of measurements, the admittance description is adapted. A nice overview of other descriptions can be found in [32].

1.1 Classical TPA methods

In classical Transfer Path Analysis (TPA) the interface forces between an active and passive component are (in)directly determined at the coupled DoFs and thereafter applied to the disconnected passive component [31]. The total response at the receiver is determined by a superposition of all contributions of the source-receiver paths (e.g. engine, exhaust, transmission, air-intake, etc.), which is valid for linear, time-invariant systems. Therefore, all potential sources and paths have to be identified and measured.

To summarise, the methods comprises the following steps:

1. A (in)direct measurement procedure for the estimation of the source excitation forces in the active components acting on the interface degrees of freedom;
2. A measurement of the transfer functions of the *decoupled* receiving structure between a point of interest and the interface degrees of freedom;
3. Application of the interface forces on the transfer functions of decoupled structure.

The source A can be described as:

$$\begin{bmatrix} \mathbf{u}_1 \\ \mathbf{u}_2 \end{bmatrix} = \begin{bmatrix} \mathbf{Y}_{11}^A & \mathbf{Y}_{12}^A \\ \mathbf{Y}_{21}^A & \mathbf{Y}_{22}^A \end{bmatrix} \begin{bmatrix} \mathbf{f}_1 \\ \boldsymbol{\lambda} \end{bmatrix} \quad (1.1)$$

The receiver B can be described as:

$$\begin{bmatrix} \mathbf{u}_2 \\ \mathbf{u}_3 \end{bmatrix} = \begin{bmatrix} \mathbf{Y}_{22}^B & \mathbf{Y}_{23}^B \\ \mathbf{Y}_{32}^B & \mathbf{Y}_{33}^B \end{bmatrix} \begin{bmatrix} -\boldsymbol{\lambda} \\ \mathbf{0} \end{bmatrix} \quad (1.2)$$

¹The displacements of the substructures can be velocities or accelerations as well, depending on the nature of the impedances or admittances, see appendix A. From here on, the dependence on (ω) will be omitted.

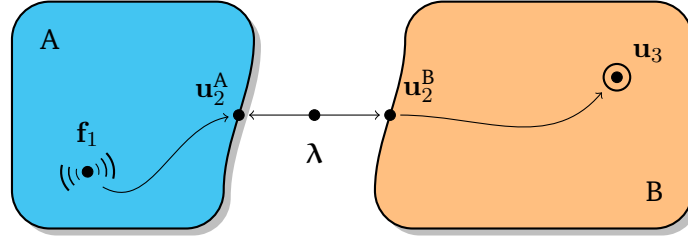


Figure 1.2: The free body diagram of the coupled structure with an acting interface force λ on the coupling degrees of freedom.

According to classical TPA, the interface forces are applied directly on the admittance of the receiving structure in (1.2), yielding to a response at a point of interest

$$\mathbf{u}_3 = -\mathbf{Y}_{32}^B \lambda$$

This result shows that the response at \mathbf{u}_3 can be physically correctly determined *if and only if* the interface forces and all other forces influencing the response are known. An expression for the interface forces can be obtained from the second line in the system of equations (1.1)

$$\lambda = (\mathbf{Y}_{22}^A)^{-1} \mathbf{u}_2 - (\mathbf{Y}_{22}^A)^{-1} \mathbf{Y}_{21}^A \mathbf{f}_1$$

which shows that the interface forces are not only dependent on the excitation in the active component A , but on the interface displacement as well. Combining this result with the expression for the interface forces in the second line in (1.2) one can express the interface displacement as²

$$\begin{aligned} [(\mathbf{Y}_{22}^A)^{-1} + (\mathbf{Y}_{22}^B)^{-1}] \mathbf{u}_2 &= (\mathbf{Y}_{22}^A)^{-1} \mathbf{Y}_{21}^A \mathbf{f}_1 \\ (\mathbf{Y}_{22}^{AB})^{-1} \mathbf{u}_2 &= (\mathbf{Y}_{22}^A)^{-1} \mathbf{Y}_{21}^A \mathbf{f}_1 \\ \mathbf{u}_2 &= \mathbf{Y}_{21}^{AB} \mathbf{f}_1 \end{aligned}$$

This result shows that both structures cannot be optimised separately as changes in either the excitation forces \mathbf{f}_1 or changes in one of the components A and B , require a renewed measurement of the interface forces, which make component optimisation extensive.

The determination of the interface forces in classical TPA methods is done via the methods as described in the following sections.

Direct Force Measurement

The first method measures simply the forces with a force transducer between the active and passive component. The use of direct force measurements are prohibitive due to the nature of the structure (difficult to place a force sensor without affecting the structure) or influencing the local stiffness of the structure by the transducer.

²The two terms can be collected as these are the point impedances of the two subsystems [13, 18]

Mount Stiffness

The *Mount Stiffness Method* can be used when the source is connected to the receiving structure with a resilient connection such that a difference in displacement between the corresponding DoFs is observable. In this case the forces can be obtained by measuring the difference in displacement \mathbf{u}_2^A and \mathbf{u}_2^B between the two connected structures and the stiffness of the resilient element $\mathbf{k}_n(\omega)$,

$$\boldsymbol{\lambda} = \mathbf{k}_n(\omega)[\mathbf{u}_2^B - \mathbf{u}_2^A]$$

Forehand knowledge is required on the (complex) dynamic stiffness of the resilient element. The characterisation of this element can be done experimentally or via a numerical model. This type of interface force determination is typically performed systems with a rubber element in the connection e.g. the engine of a car mounted on its body.

Matrix Inverse

The third method, the *Matrix Inversion Method* is used when the transfer paths include rigid connections or the connections are relatively stiff compared to the receiving structure. The relative displacements between the two structures become very small and forces can not be determined via the the mount stiffness method described in section 1.1. The operating interface forces are determined by the inversion of the accelerance \mathbf{Y}_{42}^B between a set of responses \mathbf{u}_4 (comprising the point of interest \mathbf{u}_3) at the receiver side and (impact) force excitation at the transfer path, hence with disassembled source. The interface force are determined with

$$\boldsymbol{\lambda} = (\mathbf{Y}_{42}^B)^{-1}\mathbf{u}_4$$

The number of responses \mathbf{u}_4 has to be larger than the number of forces for a sufficient over-determination. Inverse methods are widely used, in which a matrix of measured receptance is inverted at each frequency line and used with operational acceleration data to find the forces. In case of ill-conditioning of the matrix due to measurement errors, the results can often be unreliable.

1.1.1 Limitations of classical TPA methods

The classical TPA method uses techniques that are limited to measuring the transfer path of one sub-system at a time; therefore, each transfer path must be isolated in order to eliminate flanking paths. This is typically done by disassembling the system in order to make the measurements. The major disadvantages of having to disassemble the system are that the measurement process is time consuming, the boundary conditions of the sub-systems are changed, all changes to one of the both components of the structure in figure 1.1 requires a new force measurement.

As can be seen above, optimisation on the passive/receiving structure and on the excitations can not be done separately. This leads to the following observations:

- The interface forces determined in the classical TPA method are dependent on the configuration of the assembly. As a consequence, every modification to the active subsystem requires a new measurement;

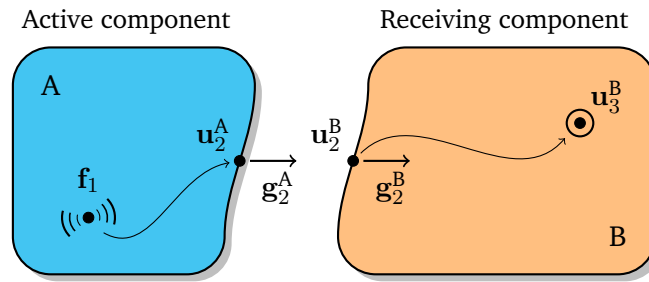


Figure 1.3: The transfer path problem based on the admittance of the substructures A and B .

- Measuring the interface forces itself, by the use of inserted force sensors at the interfaces, might influence the dynamics of the assembly, thus the interface forces. In most (complex) structures it might even not be possible to use force sensors due to the tight configuration of the systems;
- Classical TPA does not take the dynamic coupling between the active and receiving component into consideration, which is restricting the method for the use at higher frequencies [22];
- If the interface forces are to be determined on a test bench, the test facility has to fully represent the properties of the receiving structure e.g. dynamic stiffness, interfaces, otherwise errors will be made. With the use of a dynamic test bench, which represents the dynamics of the receiving structure, this problem can be overcome by Real-Time Substructuring (RTS).

1.2 Component-based TPA methods

The component-based TPA method³ attempts to characterise the excitation sources as a property of the source only. Both impedance and admittance descriptions can be used in both primal and dual coupling concepts, the interested reader is referred to [32]. Again, the admittance description is used to describe the structures. Consider the assembly AB consisting out of the two substructures A and B , illustrated in figure 1.1. The response at node 3 resulting from an excitation at node 1 at the source, is as following related:

$$\mathbf{u}_3 = \mathbf{Y}_{31}^{AB} \mathbf{f}_1 \quad (1.3)$$

The receptance matrix \mathbf{Y}^{AB} contains admittance Frequency Response Functions (FRFs) as measured on the total assembly. The set of equations in (1.3) governs the main transfer path problem. A structural modification on either the source A or receiver B requires a renewed measurement of the transfer path. Therefore, this is not a valuable way to optimise one of the structures.

In the following, the total transfer function is derived using the admittance of the individual subsystems described by their disconnected admittances \mathbf{Y}^A and \mathbf{Y}^B , as illustrated in figure

³The text in this section is based on the paper: *A robust Transfer Path Analysis method for steering gear vibration on a test bench* written by M. van der Seijs, E. Pasma, D. de Klerk and D. Rixen, submitted for presentation at the 26th International ISMA Noise and Vibration Engineering Conference (ISMA2014) - Leuven, Belgium [35]

1.3. The assembly of the two substructures is put in a block-diagonal format and extended with interface forces \mathbf{g}_2 acting on the interface DoFs of both structures and are to be determined. Considering that the system is *only* excited at node 1 of the active subsystem, the dual system reads:

$$\begin{bmatrix} \mathbf{u}_1 \\ \mathbf{u}_2^A \\ \mathbf{u}_2^B \\ \mathbf{u}_3 \end{bmatrix} = \begin{bmatrix} \mathbf{Y}_{11}^A & \mathbf{Y}_{12}^A & \mathbf{0} & \mathbf{0} \\ \mathbf{Y}_{21}^A & \mathbf{Y}_{22}^A & \mathbf{0} & \mathbf{0} \\ \mathbf{0} & \mathbf{0} & \mathbf{Y}_{22}^B & \mathbf{Y}_{23}^B \\ \mathbf{0} & \mathbf{0} & \mathbf{Y}_{32}^B & \mathbf{Y}_{33}^B \end{bmatrix} \begin{bmatrix} \mathbf{f}_1 \\ \mathbf{g}_2^A \\ \mathbf{g}_2^B \\ \mathbf{0} \end{bmatrix} \quad (1.4)$$

The upper part and lower part of the admittance matrix contain the FRFs of respectively the active and passive component. Actually, the fourth column in the admittance matrix is of no use as there is no excitation on node 3 of the receiving structure, but has been shown here for the sake of completeness. Coupling the two structures in (1.4) according to the dual assembly approach, the interface force equilibrium is satisfied *a priori* and a set of interface displacements is defined, satisfying the compatibility constraint, hence⁴

$$\text{Displacement compatibility: } \mathbf{B} \mathbf{u} = \mathbf{0} \quad (1.5a)$$

$$\text{Force equilibrium: } \mathbf{g} = -\mathbf{B}^T \boldsymbol{\lambda} \quad (1.5b)$$

$$\text{with: } \mathbf{B} = \begin{bmatrix} \mathbf{0} & -\mathbf{I} & \mathbf{I} & \mathbf{0} \end{bmatrix} \quad (1.5c)$$

The set $\boldsymbol{\lambda}$ governs the interface forces and replaces \mathbf{g}_2 such that equilibrium is automatically enforced: $\mathbf{g}_2^A + \mathbf{g}_2^B = \mathbf{0}$ and $\mathbf{g}_2^A = -\mathbf{g}_2^B = \boldsymbol{\lambda}$. The required interface forces $\boldsymbol{\lambda}$ can now be determined by enforcing (1.5a) on (1.4) and thus substituting the second and third equation of (1.4) into (1.5a).

$$\begin{aligned} \mathbf{Y}_{22}^B \mathbf{g}_2^B - (\mathbf{Y}_{21}^A \mathbf{f}_1 + \mathbf{Y}_{22}^A \mathbf{g}_2^A) &= \mathbf{0} \\ -(\mathbf{Y}_{22}^A + \mathbf{Y}_{22}^B) \boldsymbol{\lambda} &= \mathbf{Y}_{21}^A \mathbf{f}_1 \\ \boldsymbol{\lambda} &= -(\mathbf{Y}_{22}^A + \mathbf{Y}_{22}^B)^{-1} \mathbf{Y}_{21}^A \mathbf{f}_1 \end{aligned} \quad (1.6)$$

The interface forces $\boldsymbol{\lambda}$ expressed in equation (1.6) result from the operational excitation \mathbf{f}_1 inside the source component *A* and act at the coinciding interface DoFs \mathbf{u}_2^A and \mathbf{u}_2^B . The response \mathbf{u}_3^B at the receiving structure is found by substituting (1.6) into the last line of Eq. (1.4) and using the definition of Eq. (1.5b):

$$\begin{aligned} \mathbf{u}_3 &= \mathbf{Y}_{32}^B \mathbf{g}_2^B = -\mathbf{Y}_{32}^B \boldsymbol{\lambda} \\ &= \mathbf{Y}_{32}^B (\mathbf{Y}_{22}^A + \mathbf{Y}_{22}^B)^{-1} \mathbf{Y}_{21}^A \mathbf{f}_1 \end{aligned} \quad (1.7)$$

The expression for the response at \mathbf{u}_3 to an input \mathbf{f}_1 in equation (1.7) is equal to the transfer function the assembled transfer function (1.3) and is consistent to the Lagrange Multiplier Frequency Based Substructuring (LM-FBS) expression (B.5) for coupled admittances.

⁴For more information on Dynamic Substructuring (DS) and the construction of the signed Boolean matrix \mathbf{B} and both the compatibility and equilibrium condition, the reader is referred to appendix B

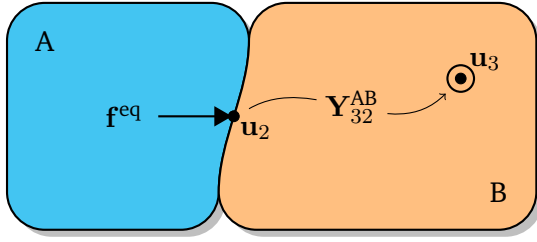


Figure 1.4: Application of equivalent forces to the interface of the assembly.

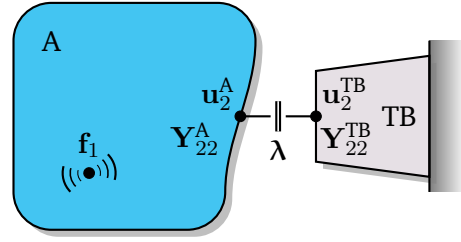


Figure 1.5: Measurement of interface forces and displacements on a test bench.

1.2.1 The equivalent source problem

The aim of this section is the identification of the internal excitation \mathbf{f}_1 in the source substructure such that an equivalent set of forces \mathbf{f}_2^{eq} at the subsystem interface is derived. The unknown excitation forces are thus modelled as a set of equivalent forces on the interface that yields the same response at receiver structure as in relation (1.3). If the equivalent forces are determined only as a property of the source component itself, the set of equivalent forces can be determined *independently* of the receiving structure. Therefore, an equivalent problem to (1.7), determined with assembled substructures, requires that:

1. A set of equivalent forces represents the excitation forces of the source component and yields to responses at \mathbf{u}_3 as in relation (1.7);
2. the equivalent forces can be identified as a property of the active component only and therefore can be characterised separately i.e. on test bench.

Conceptually, such an equivalent problem can be seen as a result of Thévenin's equivalent source theory transposed to structural vibrations. Although the concept finds its roots in electronic network theory [38] it was thankfully adopted by many structural and acoustic analysts; see for instance [30] for early derivations or [18] for an historical overview of related mobility/impedance methods.

1.2.2 Equivalent response at passive side

Analogue to the relation (1.3), that relates the operational source excitation \mathbf{f}_1 to the response at the receiver side \mathbf{u}_3 , a set of equivalent external force \mathbf{f}_2^{eq} is applied to the interface nodes of the coupled structure that yields the same response, as illustrated in figure 1.4. Thus, setting the operational forces $\mathbf{f}_1 = \mathbf{0}$ and applying the equivalent forces to the coupled structure:

$$\begin{aligned} \mathbf{u}_3 &= \mathbf{Y}_{32}^{\text{AB}} \mathbf{f}_2^{\text{eq}} \\ &= \mathbf{Y}_{32}^{\text{B}} \left(\mathbf{Y}_{22}^{\text{A}} + \mathbf{Y}_{22}^{\text{B}} \right)^{-1} \mathbf{Y}_{22}^{\text{A}} \mathbf{f}_2^{\text{eq}} \end{aligned} \quad (1.8)$$

The expansion into subsystem admittance is a similar result as seen in relation (1.7). Therefore the equations (1.7) and (1.8) need to be equal to another

$$\mathbf{Y}_{32}^{\text{B}} \left(\mathbf{Y}_{22}^{\text{A}} + \mathbf{Y}_{22}^{\text{B}} \right)^{-1} \mathbf{Y}_{21}^{\text{A}} \mathbf{f}_1 = \mathbf{Y}_{32}^{\text{B}} \left(\mathbf{Y}_{22}^{\text{A}} + \mathbf{Y}_{22}^{\text{B}} \right)^{-1} \mathbf{Y}_{22}^{\text{A}} \mathbf{f}_2^{\text{eq}}$$

it follows that the equivalent force \mathbf{f}_2^{eq} takes the form:

$$\boxed{\mathbf{f}_2^{\text{eq}} = \left(\mathbf{Y}_{22}^A\right)^{-1} \mathbf{Y}_{21}^A \mathbf{f}_1} \quad (1.9)$$

In the next section various approaches are discussed how to obtain the equivalent forces (1.9) from measurements.

1.2.3 Equivalent forces from test bench measurements

Suppose the active component A is mounted on a test bench (TB) on all its connections \mathbf{u}_2^A as visualised in figure 1.5. A comparable system of equations to (1.4) can be written

$$\begin{bmatrix} \mathbf{u}_1^A \\ \mathbf{u}_2^A \\ \mathbf{u}_2^{\text{TB}} \end{bmatrix} = \begin{bmatrix} \mathbf{Y}_{11}^A & \mathbf{Y}_{12}^A & \mathbf{0} \\ \mathbf{Y}_{21}^A & \mathbf{Y}_{22}^A & \mathbf{0} \\ \mathbf{0} & \mathbf{0} & \mathbf{Y}_{22}^{\text{TB}} \end{bmatrix} \begin{bmatrix} \mathbf{f}_1 \\ \mathbf{g}_2^A \\ \mathbf{g}_2^{\text{TB}} \end{bmatrix} \quad (1.10)$$

Again, a rigid connection of the component A on the TB is assumed. Hence, displacement compatibility at the interface ($\mathbf{u}_2^A - \mathbf{u}_2^{\text{TB}} = \mathbf{0}$) and force equilibrium between the interface DoFs ($\mathbf{g}_2^A + \mathbf{g}_2^{\text{TB}} = \mathbf{0}$) are required. The interface force and interface displacement can be written as a function of \mathbf{f}_1 :

$$\mathbf{g}_2^A = -\left(\mathbf{Y}_{22}^A + \mathbf{Y}_{22}^{\text{TB}}\right)^{-1} \mathbf{Y}_{21}^A \mathbf{f}_1 \quad (1.11)$$

$$\mathbf{u}_2^A = \left[\mathbf{I} - \mathbf{Y}_{22}^A \left(\mathbf{Y}_{22}^A + \mathbf{Y}_{22}^{\text{TB}}\right)^{-1}\right] \mathbf{Y}_{21}^A \mathbf{f}_1 \quad (1.12)$$

From here on the superscripts will be dropped to generalise the set of interface displacements and forces. The measured states obtained from operational tests on the test bench will now be indicated by $(\cdot)^*$, hence:

- Operational interface forces are denoted by \mathbf{g}_2^* ;
- Operational interface displacements are denoted by \mathbf{u}_2^* .

From the measured states at the interface, an equivalent force vector \mathbf{f}_2^{eq} has to be constructed. From the second line of the system (1.10) and the known expression (1.9), the equivalent forces can be written as

$$\boxed{\mathbf{f}_2^{\text{eq}} = -\mathbf{g}_2^* + \left(\mathbf{Y}_{21}^A\right)^{-1} \mathbf{u}_2^*} \quad (1.13)$$

In the following sections, five approaches will be discussed varying in the assumptions of the (admittance) properties of A and TB and the choice for the set of measured states.

Blocked interface force

Consider an infinitely stiff test bench, i.e. $\mathbf{Y}_{22}^{\text{TB}} = \mathbf{0}$. Under these conditions it follows that relations (1.11) and (1.12) yield:

$$\begin{cases} \mathbf{g}_2^* &= -\left(\mathbf{Y}_{22}^A\right)^{-1} \mathbf{Y}_{21}^A \mathbf{f}_1 \\ \mathbf{u}_2^* &= \mathbf{0} \end{cases} \quad (1.14)$$

consequently, the equivalent force is simply constituted by:

$$\boxed{\mathbf{f}_2^{\text{eq}} = -\mathbf{g}_2^*} \quad (1.15)$$

This set of forces \mathbf{f}_2^{eq} is also referred to as *blocked forces*. In practice, force sensors are mounted at the interface points between the test bench and the active component. Commonly, only translational forces are measured as tri-axial force sensors are used. A full 6-DoF set of collocated interface loads is thus not easily obtained. In addition, as the relative rigidity of the test bench reduces for increasing frequencies, the method is likely to perform best for lower frequencies.

Free interface motion

At the other utmost, consider an infinitely compliant test bench or no test bench at all i.e. $\mathbf{Y}_{22}^{\text{TB}} = \infty$. The interfaces are left entirely free:

$$\begin{cases} \mathbf{g}_2^* &= \mathbf{0} \\ \mathbf{u}_2^* &= \mathbf{Y}_{21}^{\text{A}} \mathbf{f}_1 \end{cases} \quad (1.16)$$

This yields the following set of equivalent forces:

$$\boxed{\mathbf{f}_2^{\text{eq}} = \left(\mathbf{Y}_{22}^{\text{A}}\right)^{-1} \mathbf{u}_2^*} \quad (1.17)$$

This method is only valid for free interface conditions, i.e. no test bench interaction. In practice one needs to suspend the active component somehow to be able to measure the interface motion at the active component under operation, for instance with soft springs. Apart from any practical issues in operating the active component in these conditions, the fact that the true rigid body modes are in practice suppressed by a suspending system, the free interface motion method is likely to perform best for higher frequencies. This method is also known as a free-velocity method.

Remark The two methods described so far represent extreme cases, i.e. respectively infinitely stiff test bench and no test bench. When applied to a single test bench setup, both methods will always yield different equivalent forces.

Combined interface force + interface motion

As can be seen from the relation of the equivalent forces a combination of the blocked force and free interface method also result in a equivalent force formulation as they are in fact complimentary:

$$\boxed{\mathbf{f}_2^{\text{eq}} = -\mathbf{g}_2^* + \left(\mathbf{Y}_{22}^{\text{A}}\right)^{-1} \mathbf{u}_2^*} \quad (1.18)$$

In this case, both the interfaces forces and interface motion are measured and combined to set up a hybrid equivalent force. Physically it can be explained that the second term compensates for the non-measured interface force due to the dynamic displacement of the test bench. This approach was earlier proposed in [23] and further studied in [9]; the latter term in (1.18) was regarded as the *non-rigid test bench compensation* (NRTB) to the original blocked-force TPA obtained by application of the first term. Indeed it can be verified that from equations (1.11) and (1.12) that (1.18) is obviously equal to the in the equivalent force written Eq. (1.9).

Matrix-inverse force + interface motion

From the third line in the system of equations in (1.10) one reads:

$$\mathbf{g}_2^{\text{TB}} = (\mathbf{Y}_{22}^{\text{TB}})^{-1} \mathbf{u}_2^{\text{TB}}$$

As the active component is assumed to be rigidly connected to the test bench, the measured interface force in equation (1.18) can be replaced by a matrix-inverse force determination based on the admittance of the TB :

$$\mathbf{f}_2^{\text{eq}} = \left(\mathbf{Y}_{22}^{\text{TB}} \right)^{-1} \mathbf{u}_2^* + \left(\mathbf{Y}_{22}^{\text{A}} \right)^{-1} \mathbf{u}_2^* \quad (1.19)$$

In this scheme, only measurements of the interface motion are required. However, separate tests should be conducted to obtain the subsystem admittances of respectively the active component A (in free conditions) and the test bench TB.

In-situ force determination

The two terms in equation (1.19) can be collected as it represents the assembly of the point-impedances of its subsystems. Therefore, it follows naturally that one can determine equivalent forces directly from the assembly of the substructures A and TB:

$$\mathbf{f}_2^{\text{eq}} = \left(\mathbf{Y}_{22}^{\text{ATB}} \right)^{-1} \mathbf{u}_2^* \quad (1.20)$$

This method has been introduced as the *in-situ* force determination in [14, 29]. Although the original derivation relies on Thévenin's and Norton's equivalent source identities, this derivation using DS leads to the same equation.

1.2.4 General remarks on equivalent force procedures

The following general remarks are noteworthy:

- It is implicitly assumed that the operational excitation forces \mathbf{f}_1 in the steering gear are independent of the global dynamics of the total system.
- The determination of equivalent forces through matrix-inverse procedures is highly prone to errors in the admittances of the subsystems involved. Over-determination of the admittances generally improves robustness, which is for example very easily performed on the equivalent force formulation in (1.20) [9]. In practice, admittances are virtual-point transformed at the right side to represent virtual point loads (see section 2.1). The set of measured accelerations do however not need to be transformed, hence an overdetermined system is easily obtained.
- Unidentified interface effects between the active and passive component are not accounted for without substantial effort, especially in case of the free interface motion method. Damping due to interface effects is a well-known aspect in the experimental DS community, see for instance [7, 8].

- Signal-to-noise ratio issues on dynamic displacement transducers are often observed in especially the low frequency region if the test bench is too stiff. Therefore, it is not a trivial choice on which method of equivalent force determination to rely, taking test bench dynamics into consideration.
- Literature on mechanical impedance / mobility methods often refers to the term $(\mathbf{Y}_{22}^A)^{-1}$ as the *parallel impedance* \mathbf{Z}_{22}^A in a Thévenin equivalent source problem [16, 18, 20]. Indeed, \mathbf{Z}_{22}^A can be determined by performing both the blocked force and free interface experiment and dividing the spectra of the (blocked) forces \mathbf{f}_2^* obtained in Eq. (1.15) by the (free) motion \mathbf{u}_2^* of Eq. (1.17). Equation (1.15) itself is then referred to as a *Thévenin equivalent source* using a force in parallel, whereas (1.17) is regarded as a *Norton equivalent source* using a motion (traditionally velocity) source in series.
- The relations (1.11) and (1.12) show that the dynamics of the test bench are the main influence on the measured states \mathbf{u}^* and \mathbf{g}^* and thus the composition of the equivalent forces.

1.3 Summary

In this chapter it has been shown that the Transfer Path Analysis (TPA) problem depicted in figure 1.1 can be replaced by an equivalent problem by the application of a set of equivalent forces on the interface of the assembly. This set of equivalent forces can be obtained by various methods which yield a test bench independent set of forces.

Chapter 2

Obtaining Dynamic models from measurements

Whereas in numerical analysis dynamic substructuring is well accepted, its experimental equivalent is far from trivial and still a topic up to today. The inability to measure all sub-system's properties for dynamic substructuring B, brings up a lot of practical issues regarding the connectivity of substructures. Some of these challenges are

1. Real-life structures are often coupled with surfaces and bolted connections, whereas Dynamic Substructuring techniques couple systems on a chosen set of degrees of freedom. This fact demands for modelling techniques for continuous interfaces;
2. Commonly, only translational degrees of freedom are measured for coupling systems. Besides translational DoFs, rotational DoFs are important as well in coupling systems. The importance of rotational degrees of freedom are regarded to be key to successful experimental DS of structures [12, 22];
3. Practically, sensor positioning on the exact location of the coupling points is challenging, as only on the surface of structures sensors can be placed, which requires for mapping techniques.

These challenges in the definition of interfaces and the connectivity between substructures have led to different solutions proposed in literature [3, 8, 22, 26]. In this work the Virtual Point (VP) transformation according to [36] is used. The method assumes that the interface exhibits locally only rigid modes, the so-called rigid Interface Displacement Modes (IDMs), on which the translational displacement or forces are projected. A key benefit of the method is that the resulting generalised motion and loads are collocated in a single point: the *virtual point*¹. Due to the nodal description, compatibility is automatically ensured with Finite

¹The point is called virtual as no actual measurement has been done in this point besides, it can be placed in an arbitrary location in the vicinity of the interface.

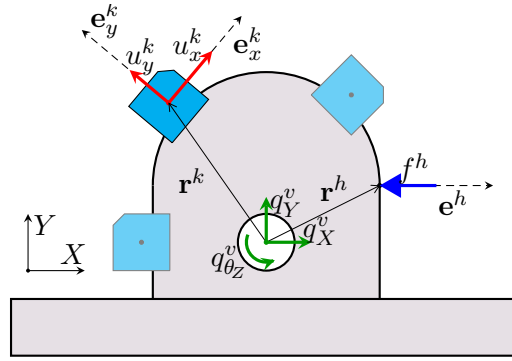


Figure 2.1: Construction of the IDMs

Element models, which makes it beneficial for numerical/experimental Dynamic Substructuring applications and structural optimisation purposes. An additional benefit of the method is the suppression of uncorrelated measurement noise due to the least-square nature of the transformation.

2.1 Theory on Virtual Point Transformation

Let us consider an interface point surrounded by N translational DoFs \mathbf{u} , as illustrated in figure 2.1. This set of measured DoFs can be reduced to M generalised DoFs \mathbf{q} by means of a kinematic mapping matrix \mathbf{R} . Since the number of generalised DoFs is smaller than the amount of measured DoFs ($M < N$), a vector of residual displacements $\boldsymbol{\mu}$ is added:

$$\mathbf{u} = \mathbf{R}\mathbf{q} + \boldsymbol{\mu} \quad (2.1)$$

If the set of reduced DoFs \mathbf{q} is chosen to describe three translations and three rotations, the columns of the matrix \mathbf{R} represent the rigid IDMs. By imposing $\mathbf{R}^T \boldsymbol{\mu} = \mathbf{0}$ the residual motion is orthogonal to the space spanned by \mathbf{R} . It can be shown that minimisation of $\boldsymbol{\mu}$ leads to \mathbf{q} as a function of \mathbf{u} by a least-squares projection:

$$\mathbf{q} = \mathbf{T}_u \mathbf{u} \quad \text{with} \quad \mathbf{T}_u \triangleq (\mathbf{R}^T \mathbf{R})^{-1} \mathbf{R}^T \quad (2.2a)$$

The virtual point loads can be determined by application of a similar mapping technique. Choosing a mapping matrix \mathbf{G} for the applied forces \mathbf{f} to virtual point loads $\tilde{\mathbf{f}}$, the transformation yields:

$$\mathbf{f} = \mathbf{T}_f^T \tilde{\mathbf{f}} \quad \text{with} \quad \mathbf{T}_f \triangleq (\mathbf{G}^T \mathbf{G})^{-1} \mathbf{G}^T \quad (2.2b)$$

The transformation of the displacement and/or excitations to the virtual point description is naturally suitable to transform measured admittances by substitution of Eq. (2.2a) and Eq. (2.2b) into $\mathbf{u} = \mathbf{Y}\mathbf{f}$:

$$\mathbf{q} = \tilde{\mathbf{Y}} \tilde{\mathbf{f}} \quad (2.3)$$

where $\tilde{\mathbf{Y}} \triangleq \mathbf{T}_u \mathbf{Y} \mathbf{T}_f^T$ denotes the collocated virtual point admittance. $\tilde{\mathbf{Y}}$ can be used for substructuring with other components, either derived from experimental or from numerical

²For a elaborated description on the construction of a set of Interface Displacement Modes, the reader is referred to [36]

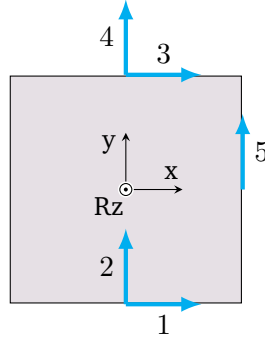


Figure 2.2: A theoretical structure with a virtual point described with 3 IDMs, observed by 5 sensors.

models, provided that the description of the virtual points is chosen such that it corresponds to the six degrees of freedom of a node.

Alternatively one may choose to perform the virtual point transformation only at one side i.e. *one-sided transformation*. Transforming the FRF matrix only on one side means that either the displacements or forces are left in their original description, for instance virtual point forces to non-transformed accelerations i.e. $\mathbf{u} = \mathbf{Y}\mathbf{T}_f^T\tilde{\mathbf{f}} = \mathbf{Y}_{um}$. In this manner an overdetermined system can be obtained, which can be exploited in the theory outlined in section 1.2.3 by the use of a pseudo-inverse of the a measured receptance matrix, see also [9].

2.1.1 A note on the virtual point transformation³

Consider the square structure (100x100 mm) in figure 2.2, of which the interface dynamics are to be described with 3 IDMs. As can be seen, the 5 channels which have to describe the virtual DoFs, point in either the x- or y-direction i.e. the odd channels are orthogonal to the even channels. Furthermore, only the odd channels exert a moment around the z-axis.

According to equation (2.1) a kinematic mapping matrix \mathbf{R} can be constructed with the sensor distances in (m). The transformation matrix \mathbf{T} is computed by the pseudo-inverse of \mathbf{R} :

$$\mathbf{R} = \begin{bmatrix} 1 & 0 & 0.05 \\ 0 & 1 & 0 \\ 1 & 0 & -0.05 \\ 0 & 1 & 0 \\ 0 & 1 & 0.05 \end{bmatrix} \quad \mathbf{T} = \begin{bmatrix} 0.5 & 0 & 0.5 & 0 & 0 \\ -0.125 & 0.375 & 0.125 & 0.375 & 0.25 \\ 7.5 & -2.5 & -7.5 & -2.5 & 5 \end{bmatrix}$$

As can be seen in the second row of the transformation matrix \mathbf{T} , the virtual point DoF in the y-direction is constructed by a combination of *all* original channels. Physically, this result does not make any sense: the virtual DoF in y-direction can *physically* not be described by original sensors orthogonal to the virtual DoF i.e. the virtual DoF is not observable by orthogonal channels.

³This section is based on an observation during the processing of a virtual point transformation. There is no definite mathematical proof given, but the observations have been verified by 'playing' with the virtual point transformation. This section should be regarded as a lead for improvement of the transformation.

This phenomena is due to the fact that mathematically speaking, the rotation R_z is over-determined by the odd channels. This results in off-diagonal terms in the $\mathbf{S} = \mathbf{R}^T \mathbf{R}$ matrix. By itself is over-determination of the rotation R_z not a problem, but the fact that the rotation is composed out of components from multiple directions (1,3:x-dir. and 5:y-dir.) make this 'cross-effect' happening.

To summarise,

The least-squares approximation yield unrealistic translation DoFs if a rotational DoF is composed out of components from multiple directions.

This observation is an interesting topic for discussion for future work.

2.1.2 Monitoring the quality

The quality of the virtual point displacements, loads and admittances can be monitored in both the pre- and post processing phase of transformation of the measurements. Here, three performance indicators in the virtual point transformation are shortly described; for more information see [36].

1. **Observability** – The mapping of the displacements and the forces on the respective set of chosen DoFs is a purely spatial transformation. It is therefore possible to evaluate the square matrix \mathbf{S} before the actual measurement has taken place. This matrix is defined as

$$\mathbf{S} = (\mathbf{R}^T \mathbf{R}) \quad (2.4)$$

To describe all generalised DoFs in \mathbf{q} , the square matrix \mathbf{S} shall be full rank and well conditioned. This condition number of the matrix \mathbf{S} , with the use of the l_2 -norm, is defined as

$$\kappa(\mathbf{S}) = \frac{\sigma_{max}(\mathbf{S})}{\sigma_{min}(\mathbf{S})}$$

where $\sigma_{max}(\mathbf{S})$ and $\sigma_{min}(\mathbf{S})$ are the largest and smallest eigenvalue of the corresponding matrix, respectively. The magnitude of the this eigenvalue gives information in how well a mode is described. For example, if there is a linear dependence in \mathbf{R} this results in a rank deficiency in \mathbf{S} see (2.4) and the condition number goes to infinity i.e. a particular VP RDoF cannot be described. Furthermore will a badly described mode i.e. small eigenvalue (two sensors placed closely together i.e. badly described RDoF) lead to error magnification of eventual measurement errors.

2. **Consistency** – To verify the consistency of the placement of the sensors and the excitation positions with respect to the IDMs, the *sensor* and *impact consistency* is used [36]. This measure is similar to the Modal Assurance Criterion (MAC) [2] and indicates how well the measured responses/excitations are described by the interface reduction through the IDMs with a value between 0 and 1. For example, the sensor consistency it is analysed how the responses \mathbf{u} are described by \mathbf{q} , with the known relation of the filtering in equation (2.2a)

$$\hat{\mathbf{u}} = \mathbf{P} \mathbf{u} \quad \text{with} \quad \mathbf{P} \triangleq \mathbf{R} \mathbf{T}_u \quad (2.5)$$

When there is no residual motion at all, the reduced set \mathbf{q} fully describe the actual set of displacements \mathbf{u} and the reduction is fully consistent. For example, if the interface spanned by the sensors show a flexible behaviour, there will be more residual motion as the IDM assumption is not valid over the entire frequency. This is reflected by decreasing sensor consistency over frequency.

The sensor consistency is preferably considered for a (combined) load case *not* in the vicinity of the virtual point, but somewhere else on the structure to observe the global response, to minimise the position uncertainty of an impact at the virtual point.

The impact consistency is a valuable tool to evaluate the position/orientation of the considered impact. One can evaluate how the virtual forces, of the considered virtual point, describe the response of a sensor channel.

3. **Reciprocity** – A measure on the quality of set a collocated receptance matrix is *reciprocity*. As both the input and output DoFs of the FRF matrix $\tilde{\mathbf{Y}}$ are collocated, this matrix should be reciprocal over the entire frequency band, hence

$$\tilde{\mathbf{Y}}_{ij} = \tilde{\mathbf{Y}}_{ji}$$

A non-dimensional, frequency dependent reciprocity value between 0 and 1 can be defined. Consider i and j as two different DoFs from the VP transformed set of DoFs:

$$\chi_{ij} = \frac{(\tilde{\mathbf{Y}}_{ij} + \tilde{\mathbf{Y}}_{ji})(\tilde{\mathbf{Y}}_{ij}^* + \tilde{\mathbf{Y}}_{ji}^*)}{2(\tilde{\mathbf{Y}}_{ij}^* \tilde{\mathbf{Y}}_{ij} + \tilde{\mathbf{Y}}_{ji}^* \tilde{\mathbf{Y}}_{ji})} \quad (2.6)$$

This formula shows the coherence of VP transformed FRFs corresponding to DoF i and j in both amplitude and phase. Reciprocity is of great importance in coupling substructures with Dynamic Substructuring (DS) [22].

2.1.3 Practical considerations

This section discusses practical issues considering the virtual point transformation. A step-by-step tutorial will be shown on how to build a virtual point interface model. It is assumed that tri-axial accelerometer sensors for the accelerations are used and an impact hammer for the force input for the FRF measurement, the measurement equipment used in this tutorial is shown in section G.

Number of sensors As the IDMs in the virtual point transformation have to describe the dynamics of the interface force in a minimal sense, an over-determination is desired i.e. ($n_u > n_q$). Theoretically six channels are sufficient but at least three triaxial sensors are needed to get a IDM with six observable DoFs as will be explained next.

Location of the sensors The sensors have to be located around the virtual point such that all IDMs are observable i.e. the triaxial sensors have to span a surface. For the rotational DoFs, this implies placement of the sensors distant enough from the virtual point for a good signal-to-noise ratio on the rotations. This is reflected in the eigenvalue in (2.4) of the corresponding DoF and the conditioning of the matrix. If the sensors are placed to far from each other, the influence of (local) flexible modes come into play. Furthermore,

the position and orientation of the sensors in the reference coordinate system have to be known. Valuable tools for determining the locations and orientations are CAD programs or more advanced localisation tools like the GOM photo Photogrammetry.

Number of impacts The same reasoning as with the placement of the sensors goes up. It is of great importance that at least 2 moment-like excitations for the determination of a RDoF VP are required, otherwise the virtual moment is not defined. Over-determination of the transformation i.e. more impacts than VP DoFs, improves the LS-approximation.

Impact Locations Again, all DoFs of the IDM have to be observable. The impacts have to span up and impacts in all three planes to describe the DoFs. One has to keep in mind that the impact vector should not coincide with the VP as moment like impacts have to be performed. In earlier studies [37] sensor-faces were chosen as impact locations as well. However, it is recommended *not* to use these locations due to e.g. overloading the sensors and detachment of the sensors.

Pre-analysis of the transformation Both displacement and impact virtual point transformations are *spatial* transformations. Therefore, the VP transformation can be evaluated *in advance* by analysing the rank and condition number of the matrix $\mathbf{S} = (\mathbf{R}^T \mathbf{R})$.

FRF measurement Once the complete measurement has been set up and the transformation is pre-analysed, the actual FRF measurement takes place.

Post-analysis of the transformation After all previous steps, the transformation is analysed by means of the the quality indicators provided in section 2.1.2.

General Remarks

The following general remarks are noteworthy on the virtual point transformation and the quality of the interface model:

- (Local) non-linearities in the measured structure i.e. impact excitation amplitude dependent FRFs degrade the interface model;
- position and orientation errors on the sensors and/or impacts ('wrong' \mathbf{T}) due to e.g. the measurement skills of the engineer influence VP model.
- If the measured structure has a complex geometry at/near the interface and sensor placement and impact locations are hard to reach, one can think of an adapter on which the sensors and/or impacts are placed. However, an adapter on the coupling point brings along uncertainties e.g. interface phenomena [7], (additional) mass-loading and influences of the dynamics of the adapter itself;

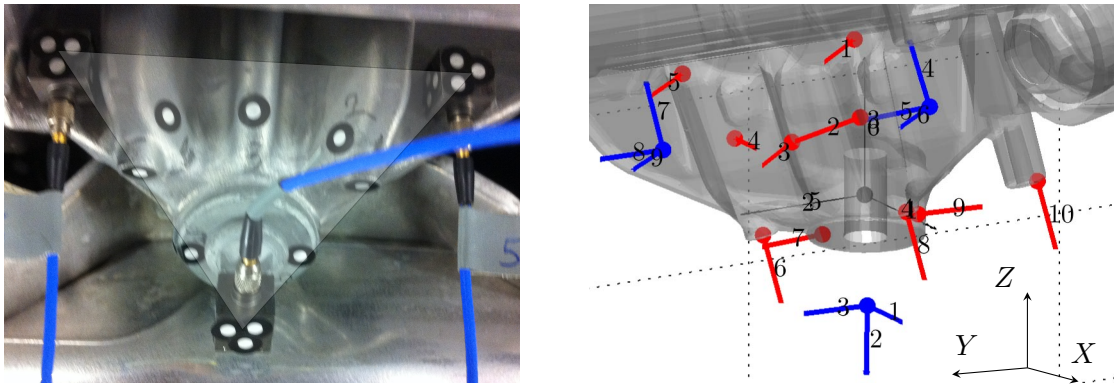


Figure 2.3: The connection point of steering gear in MATLAB and the real structure (L.). In the right figure, the virtual point is indicated in black, the sensors in blue and the impacts in red.

2.2 Example

In this section the virtual point transformation is applied to three vehicles. The transformation will be applied to a connection point of the steering gear to the vehicle. As all vehicles are identical, one expects to find similar dynamic behaviour⁴. The all steps in the virtual point transformation are analysed are discussed.

Sensor and impact location/orientation The three sensors are placed such that they span a surface and have equal distance to one another, as can be seen in figure 2.3. The ten impact locations are chosen such that they are accessed easily and can exert a 'moment' around the VP. The location and orientation of the sensors on one vehicle are determined with GOM Photogrammetry. The excitation positions are determined the the GOM system, but the orientations are determined with calculating normal vectors on that position in a CAD computer program.

The positions and orientations of the sensors and excitations on the other two vehicles are based on the positions of the first vehicle. The sensors are adhered to the structure 'on-the-eye', as-well as the positions of the excitations.

Pre-analysis of the correct location/orientation leaves little room for error and saves time in the evaluation of the VP transformation. The figures in 2.3 show the preparation of the sensor and impact locations;

Pre-evaluation of the transformation With all positions known, the IDMs can be constructed. A necessary condition for the transformation is that the matrix S is full rank equal to the number of modes, which is in this example six. Hereafter, the conditioning of the matrix is checked, but there is not such a thing as a optimum eigenvalue for a mode. In this example, the condition number of the matrix S is on the sensor-side 1403 and on the hammer-side 7060. The sensor condition number only for the rotations is 1.5, which is very low, due to the almost perfect triangle as observed in figure 2.3. For the hammer-side, the rotational condition number is 6.0.

⁴The measured vehicles are V525050, V524943 and V525963 (BMW AG internal ref.)

Perform the measurement A acceptable FRF measurement is evaluated with three checks: the coherence between multiple impacts on the same excitation location, the input spectrum of the impulse excitation and on possible overloads of a sensor. Some examples of input spectra and other important aspects of FRF measurements, the reader is referred to appendix D.1.

Post-analysis/processing After the measurement and the VP transformation, the result has to be evaluated. To evaluate the sensor consistency, the response of every sensor channel is evaluated to a combination of excitations, preferably not in the vicinity of the sensor. For example, the sensor consistency for responses of the channels 5 and 6 to a combined load far away from the coupling point, as shown in figure 2.3. A low consistency indicates that the FRF is not well described by the IDMs. This could have been caused by e.g. a position or orientation error of the, due to an overload or bad input spectrum. Therefore, the consistency can be used to re-position the sensor/hammer to optimise the transformation.

Channels in overload due to a specific excitation can be removed by the use of removing the channel/excitation from the receptance matrix, hence a full row (sensor channel) or column (impact) of FRFs. This is however a rather rigorous way of improving the model and removes possible other valuable FRFs on that specific channel/excitation. Consider the FRF in figure 2.6, the low-frequency part of the response shows unrealistic dynamics⁵. As the rest of the FRF shows reliable dynamics, the lower part of the FRF can be reconstructed with the use of modal fitting techniques as described in appendix C to (partly) rebuild the FRF. The first part of the FRF can be modelled with the pole/residue model in equation (C.4) of which the modal parameters are determined with the estimation methods described in section C. Hereafter the FRF is rebuilt with the use of a crossover function on the fitted FRF and the original measurement as can be seen in figure 2.6 as-well.

The reciprocity of the collocated virtual point transformed receptance-matrix give an is visualised in figure 2.7. In these figures the reciprocity of the virtual point DoFs of the interface model is shown. The mean reciprocity of 0-3000 Hz (l.) and 0-6400 Hz (r.) show that the reciprocity is decreases to some extent over frequency, which is due to e.g. a degrading input APS. Overall, the interface model is of good quality.

Results

In figure 2.4 the results from a standard driving point FRF (YY) and a virtual point driving point FRF (YY) are shown. In the following list, observations on the results:

- In the left plot of figure 2.4, the FRFs the three identical vehicles show equal dynamics up to ± 3000 Hz. In the upper frequency band, the FRFs do not correspond at all. On the contrary, the virtual point transformed 'driving point' FRFs shows equal dynamics of the three cars. By the use of the virtual point transformation, show that the global interface dynamics are equal on the three vehicles. Furthermore, the assumed rigid behaviour around the interface in the IDM is valid, over the entire considered frequency band.

⁵This is often observed by the use of accelerometers on structures constrained to the fixed world.

- In general, the sensor consistency is very well, which means that the IDM assumption is valid for the considered DoF. Some sensor channels show minor consistency as shown in the lower plot of figure 2.5. This is not caused by a poor position/orientation determination, as both channels in the figure belong to the same sensor. This is often observed at DoFs in a particular stiff direction of the structure.
- In the low frequency band, the virtual point transformed FRFs show overloaded behaviour. This is explained by the fact that especially at low frequencies the dynamic stiffness is very high which leads to very low values in the measured receptance, one bad FRF with a high low-frequent response (outlier), will 'pump-up' the virtual-point transformed FRF due to the LS-approximation. This phenomena can be dealt with by repairing the FRF by the use of modal fitting and approximate the low-frequent behaviour as is shown in figure 2.6. A modal fit on and the replacement of the low frequency region solves the this phenomenon.
- Even though the same transformation matrices are used for all three vehicles, based on position measurements on the first vehicle (V525050), small position/orientation errors do not propagate.
- The reciprocity of the collocated virtual point transformed FRF-matrix of one vehicle (V525050) is visualised in the plots in figure 2.7. In these figures the mean reciprocity over two frequency bands are shown, from 0-3000 Hz and 0-6400 Hz. The mean reciprocity of the receptance matrix is to some extend decreasing over frequency. This can be have several (combined) reasons
 - Position/orientation errors of the sensors/locations;
 - Little cross-coupling between some of the degrees of freedom;
 - Local (residual) flexibility i.e. rigid IDM assumption decreasing over frequency;
 - Too little over-determination;
 - Decreasing APS of the excitation force;
 - (Locally induced) non-linearities of the structure on the interface.

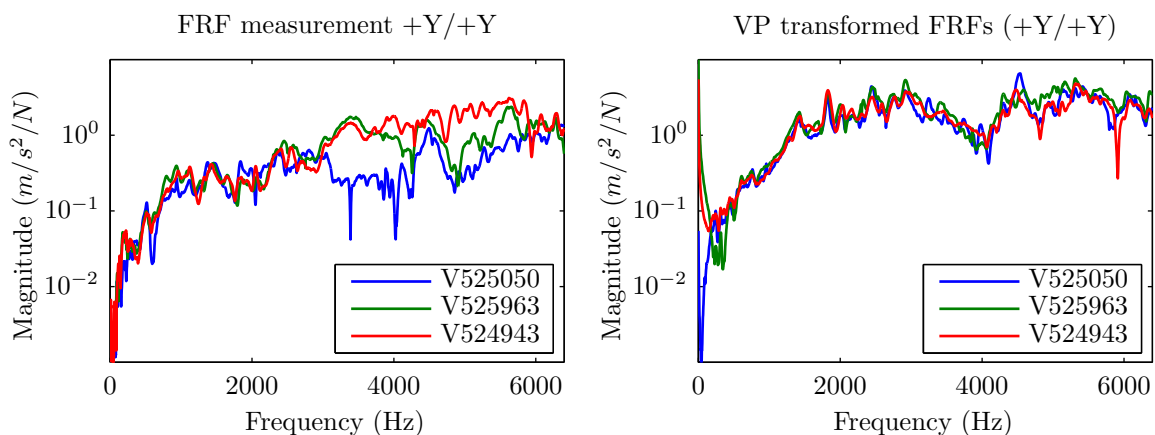


Figure 2.4: Comparison of driving-point FRFs in x -direction of three cars. On the left one can see a normal FRF, on the right side a virtual point transformed FRF.

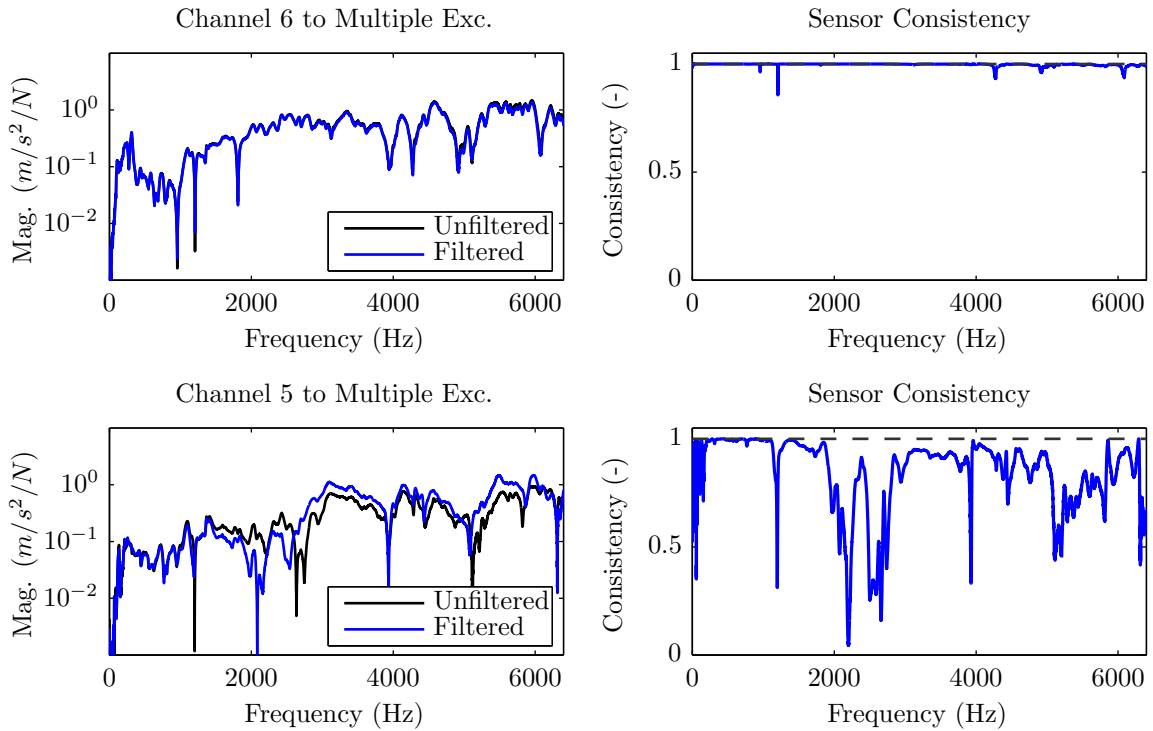


Figure 2.5: The filtered FRFs and the sensor consistency for channel 6, see figure 2.3 to a combined loadcase.

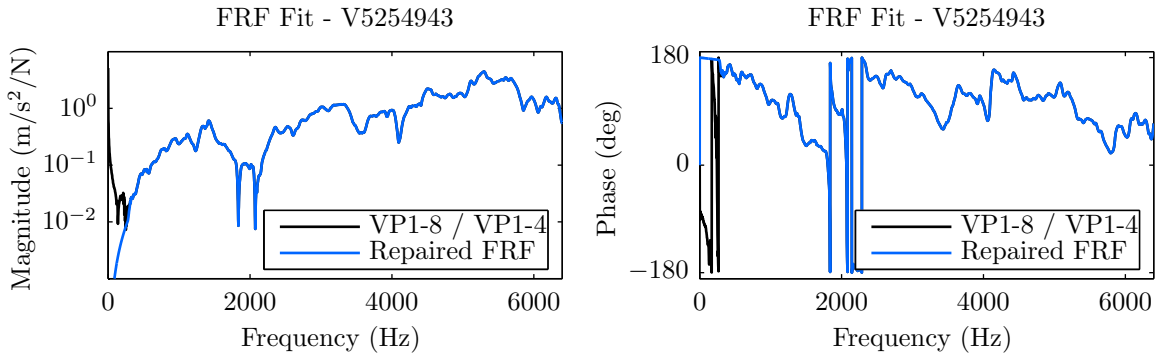


Figure 2.6: A fitted FRF for the low-frequency overload of FRF (8-4), see figure 2.3 for the FRF.

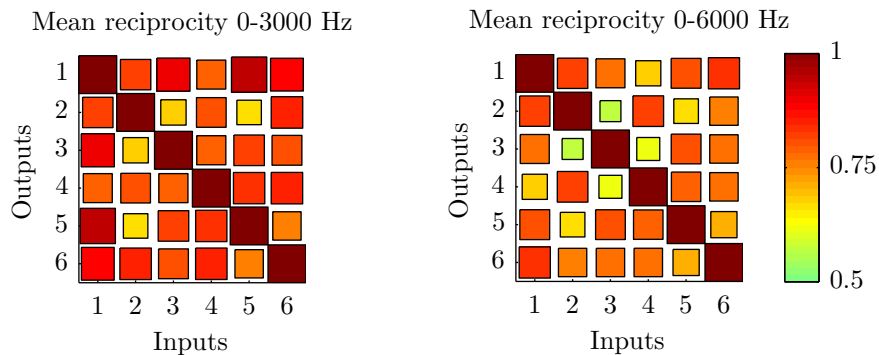


Figure 2.7: The reciprocity of the virtual point DoFs of the coupling point. The mean reciprocity of 0-3000 Hz (l.) and from 0-6400 Hz (r.).

2.3 Summary

In this chapter it has been shown that unmeasurable rotational degrees of freedom of experimentally modelled subsystems are determinable by the use of the virtual point transformation. The projection of measured Frequency Response Functions (FRFs) on local interface modes is validated by a benchmark of three equal vehicles. The individual FRFs of the vehicle do not show similar dynamics over the entire frequency band. The virtual point transformed FRFs show that the vehicles have globally equal interface dynamics. This result is valuable for the connectivity of sub-structures in the field of experimental dynamic substructuring.

Part II

Practice

Chapter 3

Industrial Test Case

The theory described in the previous chapters is addressed to a practical application. The test case comprises the structural noise contribution of a steering gear in the sixth generation BMW 5-series (F10/F11) to the acoustic experience of the driver during a typical parallel parking steering manoeuvre. First of all, the substructures and test benches are described and the test series for the steering manoeuvres are shown. Hereafter, the strategy to qualify the various equivalent force determination methods described in section 1.2.3 is rolled out.

The same notation for the structure and (interface) point will be adopted as in chapter I. For clarification the notation is summarised here

- \mathbf{Y}^{AB} assembly of the steering gear A and vehicle B or *total vehicle*;
- \mathbf{Y}^{ATB} assembly of the steering gear A and test bench TB ;
- \mathbf{f}_1 the excitation forces;
- \mathbf{u}_2 interface nodes;
- \mathbf{u}_3 the point of interest i.e. the driver's ear in the vehicle.

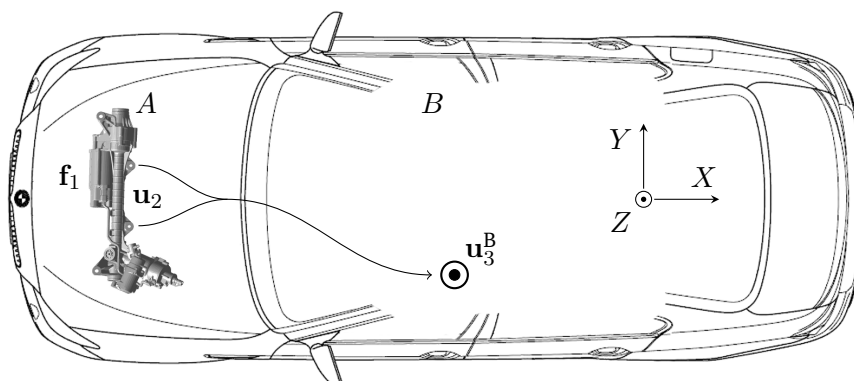


Figure 3.1: A schematic overview of the vehicle, the steering gear, the excitation \mathbf{f}_1 forces and the interface \mathbf{u}_2 and reference nodes \mathbf{u}_3 . The considered dominant transfer path through the bolted connections is indicated by the line with arrow head.

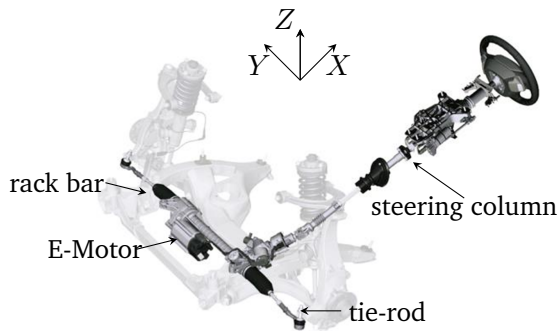


Figure 3.2: The complete steering system mounted on the subframe.

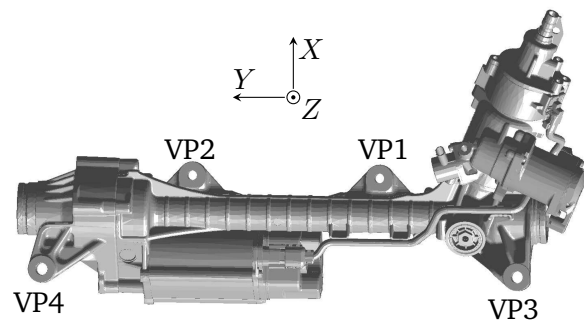


Figure 3.3: A top view of the steering gear and its considered transfer paths.

3.1 System description

In figure 3.2 the steering gear bolted to the subframe is shown. The most important parts are indicated with arrows. All its interface points, i.e. virtual points are indicated with VP1, VP2, VP3 and VP4 will be modelled with six modal degrees of freedom. Here, all structures in the TPA analysis and the test benches are described

The total vehicle the point of interest u_3 is the sound pressure level at the driver's left ear, see figure 3.1. A subframe is bolted to the chassis of the car to carry components such as the engine, drive-train, suspension and steering gear. The steering gear transfers via the subframe/chassis of the vehicle its disturbances to the driver's ear via its structural/acoustic transfer path. Direct acoustic influences are not considered.

The steering gear The electric power steering system (EPS) or steering gear is an EAS 12V model which assists the driver by augmenting steering effort of the steering wheel. Sensors detect the position of the steering wheel and the torque in the steering column to control the amount of torque provided by the electric motor which is connected via a transmission belt to the rack-bar. As e.g. the electric motor, belts and bearings are the vibration inducing elements in the vehicle, the steering gear contains f_1 .

The steering gear is on seven points mechanically connected to the subframe of the vehicle. It has four bolted connections to the subframe of the car, two tie-rods which are double ball-jointed to the kingpin and a spindle through the steering column to the steering wheel. Previous studies show that the four mounting points are the dominant paths of structural vibration [9] and are thus the considered coupling points in this thesis, hence u_2 . See figure 3.1 for a schematic overview of the car and the dominant transfer path.

3.2 Test Benches

The equivalent interface forces resulting from the internal excitation forces in the steering gear are determined by measurements on a test bench, as depicted in section 1.2.3. In the relations (1.11) and (1.12) it is observed that the dynamic properties of the test bench influence the measured states \mathbf{g}_2^* and \mathbf{u}_2^* . Regardless which method for the determination of \mathbf{f}_2^{eq} is chosen, it is of great importance that the measured states have a good signal-to-noise ratio (SNR). For example, an accelerometer on a very stiff structure has a low signal compared to the level of background noise. The opposite applies to force sensors i.e. a force sensor adhered to a free-floating structure will only measure noise. These described examples are depicted in the extreme cases (1.14) and (1.16).

In earlier TPA studies [9, 35] on the steering gear noise propagation, the *blocked interface force* method was exploited according to (1.15) on test bench **TB1**. This test bench is used in this study as well with equal methodology. In comparison to the earlier studies, the force generation on the rack bar is to some extent optimised.

Based on the results in [9] and preliminary studies in this project, it was decided to design a more compliant test bench **TB2**. The idea is to improve the SNR to both improve the admittance \mathbf{Y}^{ATB} for the *in-situ* equivalent force determination according to (1.20) and the measured operational interface accelerations on the test bench. Contrary to TB1, it was chosen to design a-symmetrical supports to reduce the effect of double eigenfrequencies. To reduce possible interface effects [7], it is chosen *not* to equip TB2 with force sensors. Furthermore, a new design of the supports of the steering gear, gave the opportunity to apply 'all lessons-learned' of the virtual point transformation and optimise the structure for the placement of sensors and impact excitation points.

In appendix F is elaborated on both the design and the construction of both test benches. Furthermore, in figure F.3 the dynamic stiffnesses of the supports VP1 and VP3 of both test benches are compared.

'Rigid' Test bench - TB1

The steering gear is mounted on four steel cylindrical supports all fitted with a tri-axial force sensor and 4 tri-axial accelerometers, see figure 3.4; The forces on the tie-rods of the steering gear are induced by the wheels turning on a concrete slab. A mass and a force balancing bridge are used to simulate the full load of the car on the front suspension. To summarize:

- Steel cylindrical supports;
- Measure 'blocked' interface forces with a tri-axial force sensor;
- Measure accelerations, 4 tri-axial accelerometers;
- Rack bar forces are generated by a modified Front Axle Carrier and wheel suspension.



Figure 3.4: A rigid support of TB1.

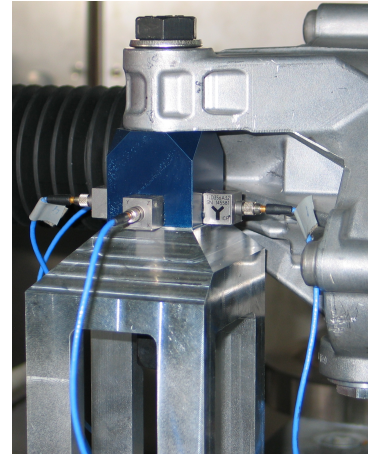


Figure 3.5: A compliant support of TB2.

'Compliant' Test bench - TB2

The steering gear is mounted on four compliant, a-symmetrical aluminium supports, see figure 3.5. These supports are not fitted with force sensors, but only with four tri-axial accelerometers to determine the interface force with the *in-situ* method. To summarize:

- Asymmetrical alluminum supports, 1 order more compliant than TB1, see figure F.3;
- Measure accelerations, 4 triaxial accelerometers;
- The forces on the rack bar exerted by hydraulically controlled cylinders.

3.3 Operational Conditions

As stated in the intro of the section, the considered operational conditions are typical parking manoeuvres. This comes down to turning the wheels to their maximum angle at 0 km/h forward vehicle speed. The **angular steering-wheel velocity is 600 deg/s**. The angular steering wheel velocity result in a rack-bar from 120 mm/s through the rack and pinion ratio of 0.2 mm/deg. One steering manoeuvre is defined as steering from right (-400°) to left (400°). To exclude any effect of the direction of steering, only steering to the right is considered. Furthermore, a steering servo motor is used to execute both steering speed and rack-bar position, to produce reproducible operational conditions. A typical steering cycle is shown in figure 3.12. The same steering profiles are used for both the validation measurement in the vehicle as on the test benches.

It is chosen only to consider this 600 deg/s steering manoeuvre as this is the optimal compromise between signal-to-noise on the sensors, the length of the measurement time-block and the limitations of the steering gear. All tests have been performed at room-temperature.

3.4 Operational rack bar forces

Due to the kinematics of the steering/suspension, the forces in the rack bar (over the distance the rack bar travels) do not depend linearly on the steering speed. The wheels do not remain flat in the XY plane and therefore lift the car to some extent when steering towards the end-stops. A typical force profile in the rack bar is shown in figure 3.12. On both test benches, the forces on the tie-rods are exerted in a different manner, hence

TB1: All mechanical components in of the steering system are present. Therefore, similar force profiles are observed compared to true steering, see figure 3.12 on page 41.

TB2: As previous analyses have shown that steering speed is the dominant variable on the noise level in the vehicle, it is chosen to control a constant force on the rack bar on TB2. This constant forces on the tie-rods on TB2 are chosen such that they match to the forces measured in the tie-rods on TB1. The constant force on the rack bar of the steering gear on TB2 are 2,5 kN. Another advantage of a constant force profile is that a steady state operation is created as much as possible for the Fourier transformation of the operational states to the frequency domain.

Making an extensive analysis with a vast variety of variables (e.g. steering speeds, rack bar forces and temperature etcetera) to study these influences and for example harmonical behaviour of the steering gear, goes beyond the scope of this thesis.

3.5 Validation strategy

In this section an outline is given for the validation strategy of the noise prediction of the steering gear vibrations to the driver's ear. The full process of modelling the dynamics of the subsystems, to the application of the equivalent forces to the total vehicle model, is visualised in figure 3.6. The validation strategy can be summarised in the following steps:

1. **Component models:** The first step in the analysis is to build a dynamic description of the structures i.e. mY_{22}^{ATB} , Y_{23}^{AB} . In this work, the models are extracted from FRF measurements on which the virtual point transformation is applied for the nodal connectivity. The models will be analysed with the use of the quality indicators described in section 2.1.2.
2. **Operational conditions:** The operational forces are mainly determined by the steering speed (600 deg/s) and the rack bar force (2,5kN). A challenge is to create true reaction forces on the rack bar on TB1, which are dependent on the friction of the wheels on the road and the kinematics of the steering/suspension. As all structures are modelled in the frequency domain, it is desired to have a steady state operational excitation. Therefore, only a short time block is extracted from the full steering manoeuvre. It will be analysed if reproducible operational interface responses can be achieved.

The operational interface equivalent forces f_2^{eq} are to be determined on the two test benches TB1 and TB2, according to the theory in section 1.2.3.

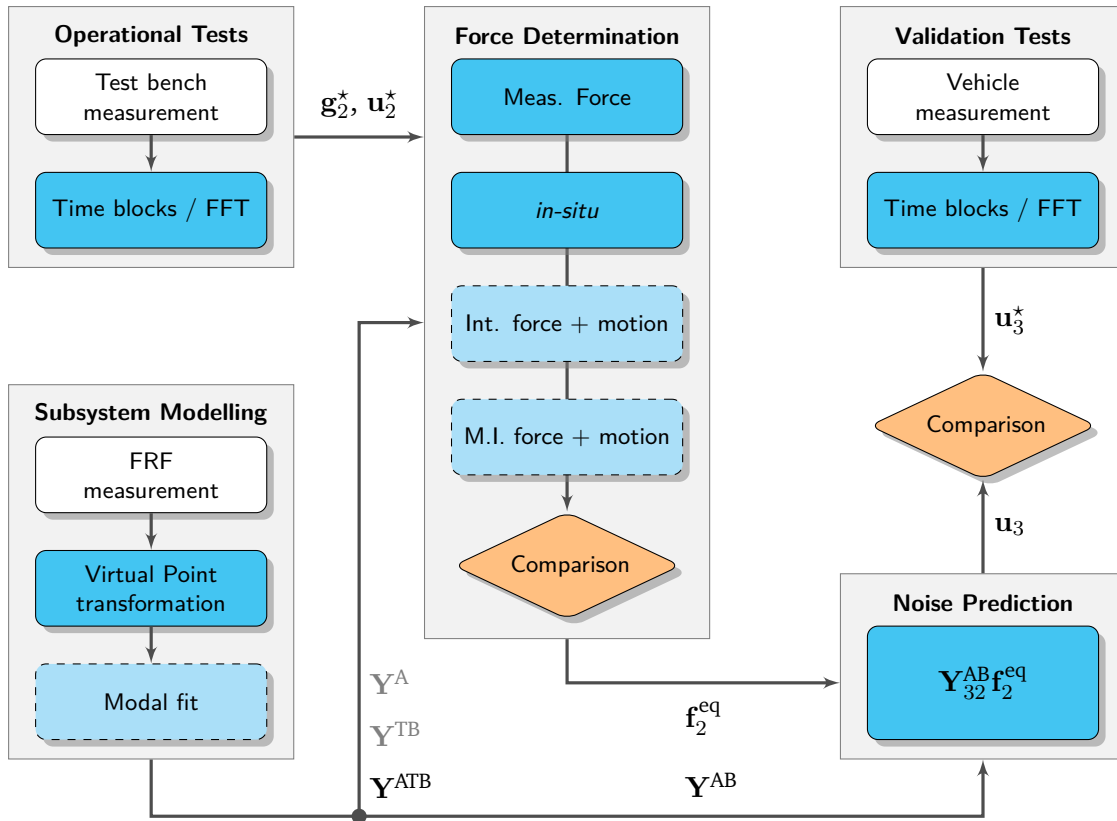


Figure 3.6: The method described in section 3.5 depicted in a flowchart.

3. **Equivalent forces**; After the modelling of the structures has been performed and the virtual point transformation has been applied for a nodal description at the interface, the equivalent forces can be determined. On the two test benches the following methods are explored:

f_2^{eq} on TB1:

- the measured interface forces g_2^* according to (1.15);
- the *in-situ* according to (1.20).

f_2^{eq} on TB2:

- the *in-situ* method will be applied.

After the determination of f_2^{eq} , the methods and the two test benches will be compared.

4. **Noise Prediction**; The equivalent interface forces f_2^{eq} , will be applied to the interface of the total system i.e. Y_{32}^{AB} according to equation (1.8). These results will be discussed and the synthesised response is compared to the validation measurements.

3.6 Application

The method outlined in the previous section is applied to the test case in this section. Due to the large number of components, complex structures and variety of materials it is fairly impossible to model all substructures numerically at higher frequencies. Therefore, all substructures are experimentally determined with measurements. In section 3.6.2 the mechanical-acoustical FRFs of the total vehicle will be described. The sections 3.6.3 and 3.6.4 the component models of the steering gear mounted on TB1 and secondly TB2, are determined and discussed. All three component models, \mathbf{Y}_{32}^{AB} , \mathbf{Y}_{22}^{ATB1} and \mathbf{Y}_{22}^{ATB2} , are measured and processed in an equal manner. Therefore, it is chosen to discuss the \mathbf{Y}_{22}^{ATB2} in depth. The other measurements are shortly described and only odd observations will be mentioned.

Section 3.6.5 considers the operational measurements. The operational measurements are performed in the time domain and thus have to be transformed to the frequency domain with the Fourier transformation. This signal processing needs to be performed carefully to address problems like e.g. spectral leakage. Hereafter, in section 3.6.6 the equivalent forces are calculated and discussed. As outlined in section 3.5, two types of equivalent forces determination schemes are used, hence the *blocked interface force* and the *in-situ* methods. The first method only requires the model of the total vehicle AB . The *in-situ* methods rely on the inverse of the steering gear and the relative test bench. Finally, in section 3.6.7 the complete TPA analysis is performed and the results are compared to the validation measurements.

In table 3.1 details of both the component modelling as the operational measurements are summarized.

component modelling

Coupling nodes:	4 virtual points
Virtual point:	6 rigid IDMs (6 DoFs)
	4 accelerometers (12 DoF)
Force measurement:	3D force sensors (TB1 only)
Validation nodes:	4 microphones (4 DoF)
Force excitation:	impact hammer, impulse signal

operational measurements

Time block	1 second
Sampling rate	16384 Hz
FFT settings	low-pass filter (<i>Butterworth</i>) at 6400 Hz
	<i>Hanning</i> window function
Repetitions	5 sequential measurements
Steering speed	600 deg/s to the right (-400 deg)
tie-rod force	2,5 kN

Table 3.1: Details on the measurements, the measurement equipment is shown in appendix G.

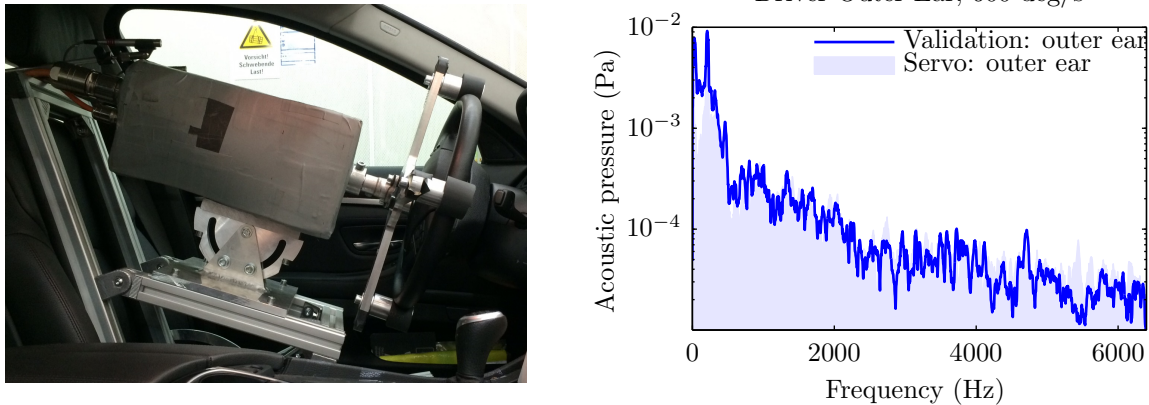


Figure 3.7: *Performing the validation measurement with the steering robot (l.). The operational acoustic pressure (r.) at the driver's ear due to a 600 deg/s steering manoeuvre at 0 km/h.*

3.6.1 Validation Measurement

The validation measurement of the operational steering gear is performed on a standard F10 vehicle with a Rexroth servomotor, controlling the steering speed and angle. The measurement takes place at standstill i.e. 0 km/h under natural boundary conditions i.e. all tyres on concrete slabs, windows closed and all seats in standard position. All systems in the vehicle are switched off. The steering gear is externally connected to a power source and to an IXXAT FRC-EP150 Flexray/CAN Box to activate the steering gear.

As the band of interest is over 6 kHz, the positioning of microphones has to be done with precision when comparing the synthesised response to the validation measurement. The wavelength λ of a sinusoidal waveform travelling with speed v (343 m/s at 20°C, $1 \cdot 10^5$ Pa for air) and the wave frequency f is related through $\lambda = v/f = 343/6400 = 53.9$ mm. Considering this result, the acoustic pressure measured with the microphone is very spatially dependent on its position. This fact has to be taken into consideration when comparing acoustic responses from different measurements.

In figure 3.7 the validation measurement is shown together with an acoustic (noise) measurement of the steering robot under the condition that it is not attached to the steering wheel. It can immediately be observed that the operational acoustic pressure at the driver's ear is completely dominated by the noise of the servo. As a consequence, this measurement with the steering robot is of limited use as a validation measurement as there is only little signal (0 - 600 Hz) over the servo noise. The optimisation of SNR problems is also recommended for future research.

3.6.2 Total vehicle FRF Measurement

The dynamics of the total vehicle \mathbf{Y}_{22} and \mathbf{Y}_{32} are measured with an impulse hammer at room temperature in an laboratory with acoustic isolation panels on the walls. The vehicle is again measured with natural boundary conditions i.e. all tyres on the ground, windows closed and all active systems shut down. The measurement comprise mechanical-acoustic FRFs of the total vehicle from the 4 interface points to 2 microphones at the driver's ears. All virtual

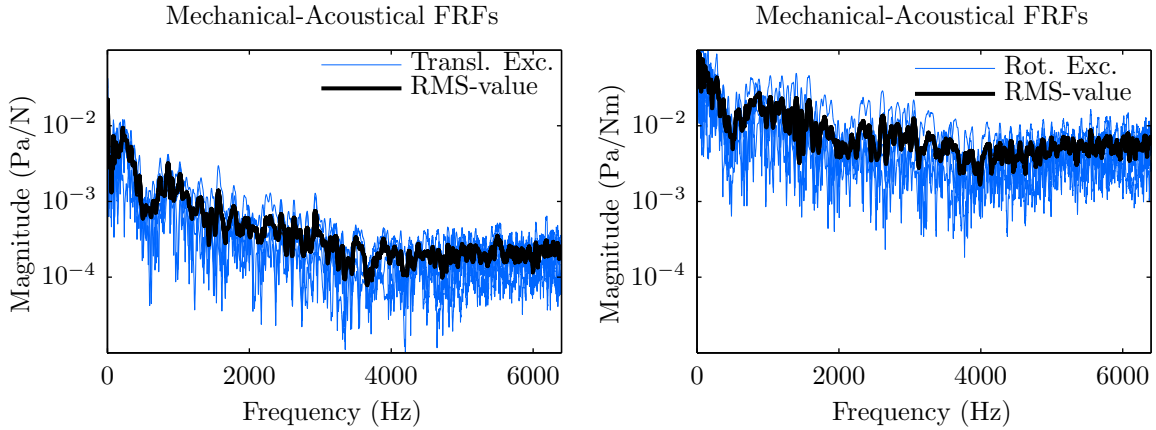


Figure 3.8: The mechanical-acoustical FRFs of the total vehicle. The translational (*l.*) and rotational (*r.*) FRFs are separated, the RMS-value of the FRFs is shown in black.

points are described by 6 DoF translational and rotational rigid IDMs. It is not required to use measurement equipment (accelerometers) at the interface. As the equivalent forces \mathbf{f}^{eq} are applied to this model, the reference channel side of the FRF matrix has to be virtual point transformed i.e. \mathbf{Y}_{um} . Therefore, the matrix has dimensions $\mathbf{Y}_{23}^{\text{AB}} = [2 \times 24 \times 6400]$.

In figure 3.8 the mechanical-acoustical FRFs are shown. The translational and rotational excitations to the microphone at the outer driver's ear are separately shown. To look at the the average of the signals, the Root Mean Square (RMS) of the FRFs is calculated through the relation, with number of measurements N :

$$P_{\text{RMS}}(\omega) = \sqrt{\frac{1}{n^2} \sum_{n=1}^N |p_n|^2}$$

The following observations are made:

- **Observation:** All translational/rotational mechanical-acoustical FRFs of the total vehicle are in the same order of magnitude. The rotational excitations yield to acoustic pressures which are about one order larger than the translational FRFs, which can be seen in figure 3.8.

3.6.3 Test bench TB1 + steering gear

The equivalent force determination with the use of the *in-situ* method requires a model of the test bench with the steering gear attached. As can be seen in figure 3.9 the supports of the test bench are equipped with 4 3D accelerometers and a 3D force sensor. The 4 accelerometers describe the virtual point displacements well and the transformation matrix is full rank and well conditioned.

- **Observation:** The 10 impact locations for excitation per virtual point did not yield to a full rank \mathbf{S} matrix. With the chosen set of impacts on a virtual point, it is not possible to describe the rotational IDM DoFs RX and RY.

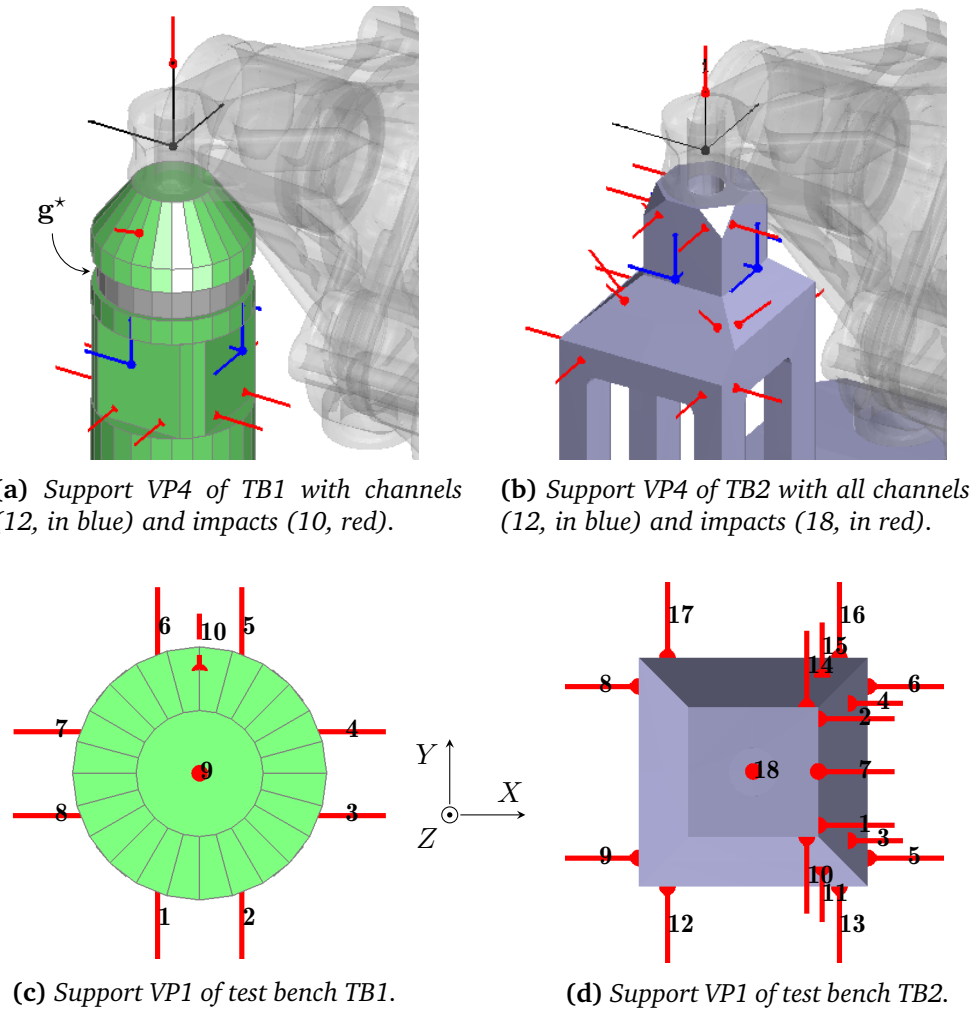


Figure 3.9: Zoom in on the measurement positions of both test benches. The virtual points are indicated in black and its axes lay in the directions of the global reference frame.

Explanation: Rank is described as the largest collection of linearly *independent* rows (or columns). Physically, this means that some of the collection of hammer impacts describe exactly the same. The impact locations on support VP1 are visualised in figure 3.9c. Indeed, it can be seen that the impacts (1-6), (2-5), (3-8), (4-7) result in equal rows in the \mathbf{R} matrix, yielding to linear dependent rows. A possible idea is to build the transformation matrix \mathbf{T}_f per IDM DoF, as the hammer excitations describe all individual IDM DoFs. The consequences of this assumption is not studied here.

3.6.4 Test bench TB2 + steering gear

Again, the in-situ method is applied for the equivalent force determination. Figure 3.9b shows one of the supports of the test bench, which are all equipped with 4 3D accelerometers. The virtual forces are determined with the transformation of 18 force impacts on the top side of the support, as can be seen in figure 3.9b and 3.9d. As only the force-side of the FRF-matrix

is to be virtual point transformed for the connectivity to the total vehicle model, there will be focussed on this reduction step. The majority of the filtered impacts are consistent in the full band and the virtual point transformed FRF matrix is very reciprocal. Observations

- **Observation:** The Hammer IDM filtering shows for some impact bad consistency in the lower frequencies (0-100 Hz), see figure 3.10.

Explanation: The low frequency behaviour is explained by cross-talk between the sensors¹. This effect can be clearly seen when evaluating a (near) driving point accelerance FRF, of which the phase should be 180 degrees, which is obviously not the case. These types of types of deficiencies can be repaired by modal fitting of the corresponding FRF in the low frequent area. Normally, no more that one pole is necessary to make a decent estimation of the response. With the use of the techniques described in appendix C, the FRF is repaired, see figure 3.11.

- **Observation:** Some filtered impacts show decreasing consistency from 4000-5000 Hz.

Explanation: The broader drops in consistency between 3500 - 5000 Hz are mainly caused by impacts in the very stiff Z-direction to or at some cross FRFs i.e. channel X - reference channel Y. Another explanation of reduced consistency is that due to the force input spectrum, which is decreasing over the frequency, a FRF is badly determined, see appendix D.

- **Observation:** The rapid 'spurious' drops in consistency are caused by anti-resonances of the structure. In the low frequent area this is mainly caused by the dynamics of the by springs decoupled test bench, on which the supports for the steering gear are mounted.
- **Observation:** The matrix S of the hammer transformation is of rank 6 i.e. all DoFs of the IDM can be described. The transformation matrix T adds up the contributions of individual channels to build a virtual point DoF, minimising the error. It is interesting to observe that, because all channels of the sensors point in direction of a DoF of an virtual point, that channels orthogonal to a VP DoF can contribute to that channel, which is counter-intuitive and physically not true, see section 2.1.1.

¹These particular ICP accelerometers are grounded via their titanium housing. Furthermore, the grounds are connected with eachother via the modules of the PAKII measurement system. It has been observed throughout the entire project that this causes large bias-errors in the 0-100 Hz frequency band.

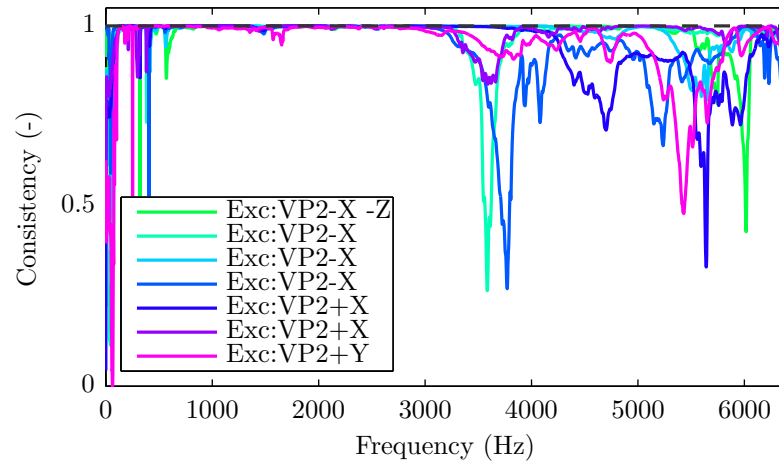


Figure 3.10: Hammer consistency of VP2 evaluated on 3 sensor channels (XYZ).

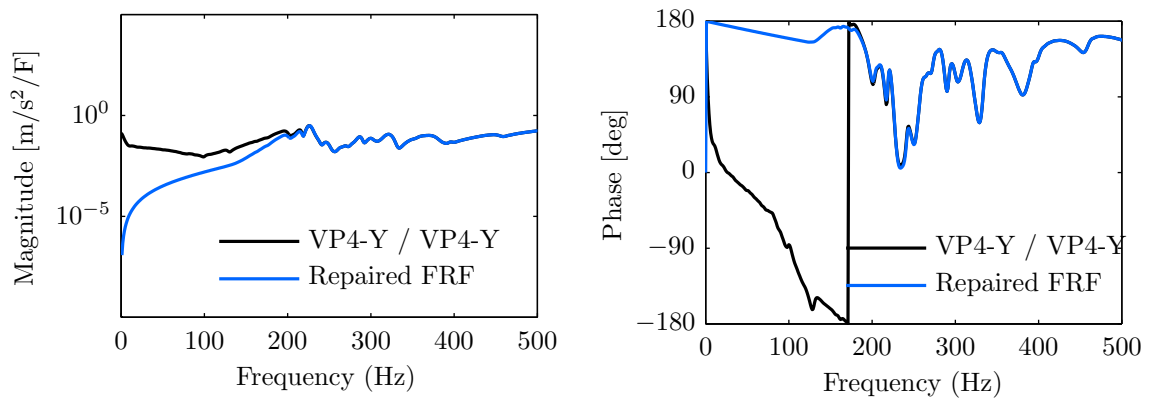


Figure 3.11: An repaired FRF with the use of a modal fit with 1 pole at 226 Hz. The FRF fit and the original FRF are fused together with the use of a cross-over function.

3.6.5 Operational Measurements

For reproducible steering gear excitation measurements on the test bench, a steering robot is used. As described in section 3.3, the operational input for the steering gear is a 600 deg/s angular velocity at the steering wheel. In figure 3.12 the most operational states of both test benches are shown. The steering robot is position controlled, therefore there is not targeted steering wheel speed, but is calculated with the time derivative of the position. In the top right graph, a typical tie-rod force parking manoeuvre curve is shown, which is non-linearly related to the steering angle due to the kinematics of the suspension of the vehicle. The two lower graphs of figure 3.12, the tie rod/rack bar forces on both test-benches are shown. As can be seen, test bench TB1 show a similar profile when steering to the right. The measurement equipment on the test benches is equal and in the same position as when performing the FRF measurements described in the above. The most important operational settings are shown in table 3.1.

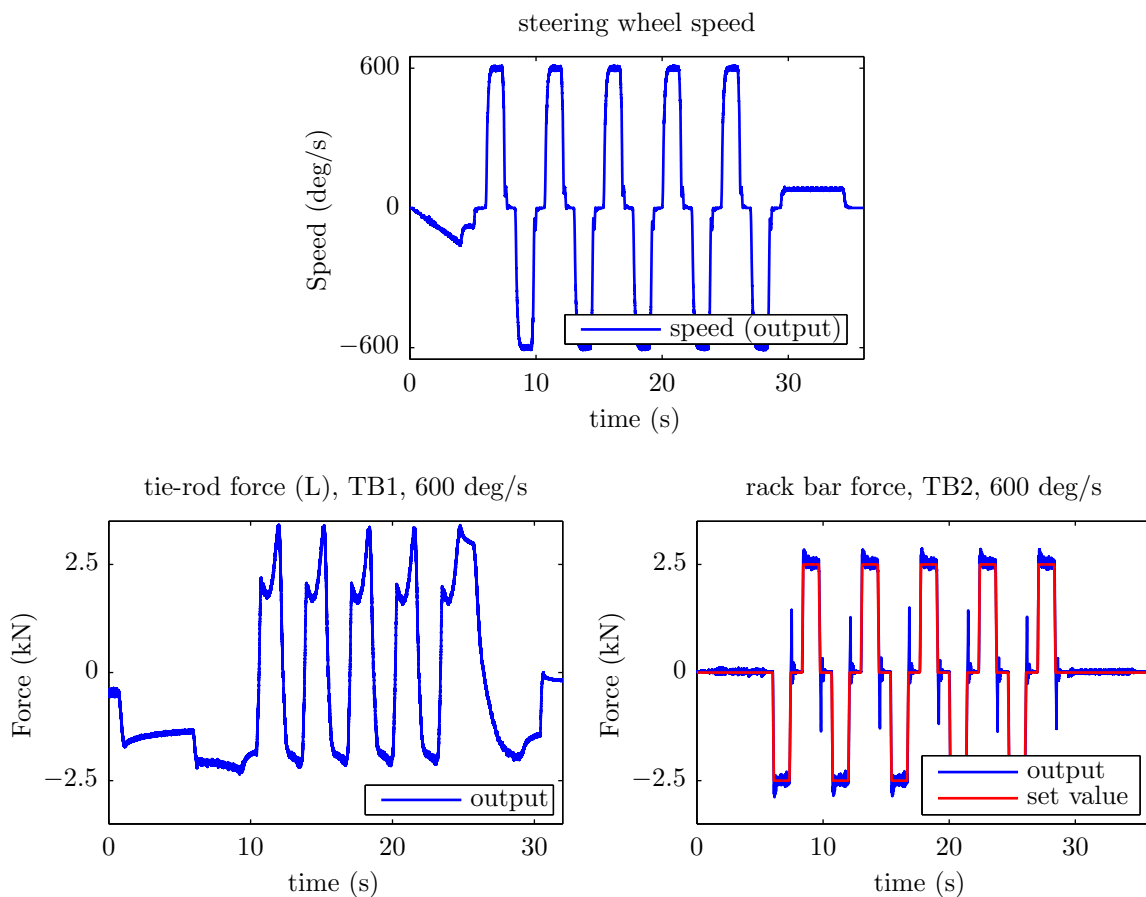


Figure 3.12: Operational states from both test benches.

The predictive analysis of the transferred vibrations to the driver's ear is performed in the frequency domain. Therefore, an important aspect in comparing sequential measurements, is the start of the time block. At the test bench TB1 there is no synchronisation available between the start of steering operation and start of the measurement. Therefore, the time blocks have to be cut out 'by hand'. The measured force in the tie-rods is used as a reference

for the start time. Test bench TB2 has communication capabilities and is able to trigger the measurement system, which simplifies the measurement time block extraction. For the validation measurements in the vehicle the same procedure is followed.

Besides all operational measurements, a noise measurement is performed. The amount of noise on the interface force/acceleration is measured with all systems active (i.e. steering gear, steering robot and force actuators), but not operational. This measurement will be used as a noise floor to which the operational measured quantity are compared.

Operational excitations

In figure 3.13 the force and acceleration spectra are shown for some randomly picked channels on both test benches TB1 and TB2, in all plots the noise floor is shown as well. The following observations can be made:

- The 5 measurement cycles are plotted in the figures in 3.13. It is easily observed that all driving cycles are very reproducible.
- In the acceleration spectrum of TB1 VP3 in figure 3.13c large peaks are observed. These peaks in the acceleration spectrum are caused by the eigen-frequencies of the assembly of test bench TB1 and the steering gear. Examining the Complex Mode Indicator Function (CMIF) of the assembly as is shown in appendix F, the eigen frequencies of the system in the XY-plane can be easily identified, which are indicated with the dashed lines in figure 3.13c.
- A sharp peak at 4000 Hz on TB1 is observed as can be seen in the figures 3.13c - 3.13b. This peak in the noise floor has been identified with the frequency at which the servomotor controls the steering actuation. This is a clear example of the disturbances of surrounding systems on the a test bench that influence the measurements severely.
- The measured forces on TB1 in the figures 3.13a - 3.13f show a downward going trend. In contrary to the acceleration spectra, the forces do not clearly show dynamics of the supports. At all 4 supports at 240 - 480 and 720 Hz clear peaks are observed in the Z-direction of the force spectra, which is probably caused by some engine orders in the steering gear system however, the in depth interpretation of the system is out of the scope of this thesis.
- On test bench TB2 the acceleration spectra are less driven through the dynamics of the TB2 + steering gear. This is also explained by the dynamic behaviour of the assembly itself, as illustrated in the CMIF in which less dominant resonance frequencies are observed, see figure F.5 on page 78.
- The signals on both test benches show an signal-to-noise ratio of 1 order. However, this ratio starts declining at about 4000 Hz and noise becomes more dominant. As expected, TB2 shows a higher signal (on average 5 times higher). Both test benches show quite dominant noise in some frequency bands, again mostly in the higher frequency area.
The noise of the surrounding systems on the force sensors, shows a 'quieter' behaviour, as the forces signals itself. Over the entire frequency band, the signal-to-noise ratio is about one order.

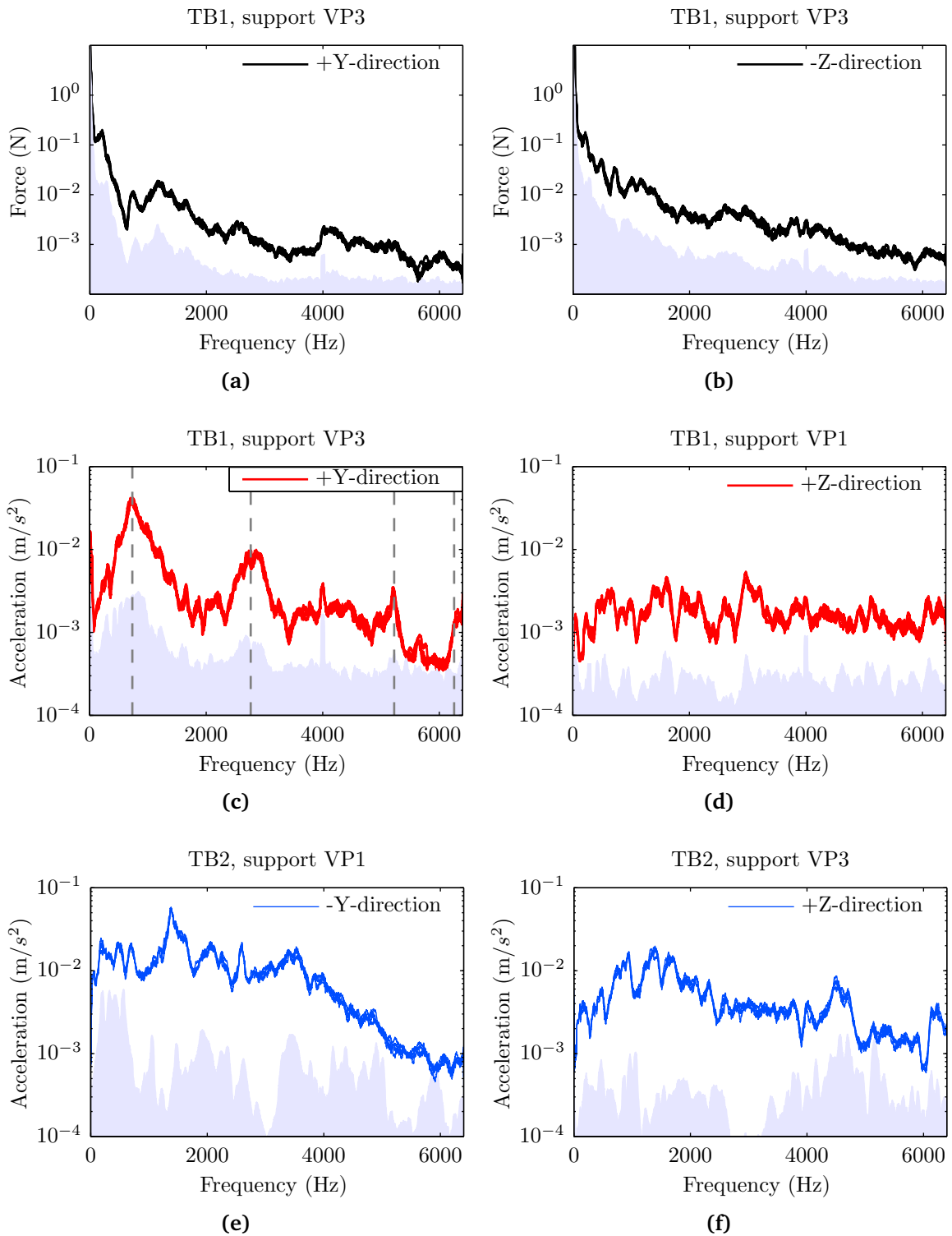


Figure 3.13: Acceleration and force spectra of several randomly picked channels on both test benches. The 5 sequential measurements show high reproducibility.

3.6.6 Equivalent forces

The equivalent forces are determined on both test-benches via the direct force measurement and the *in-situ* method. As known, the measured forces should represent true interface/equivalent forces in the case of a fully rigid test-bench i.e. no further process is required to determine the equivalent forces. The *in-situ* method however, did require a two-stage measurement to obtain all necessary data for the equivalent force determination such that the source is independently characterised. All measurement equipment i.e. accelerometers and force sensors are located at the same position/orientation as in the component modelling phase. This fact makes it possible to solve equation (1.20) in an over-determined manner with the *pseudo-inverse*. If the measurement equipment would not have been in the same position, the virtual point transformation has to be used on the channel-side of the FRF-matrix, yielding collocated operational excitations and interface dynamics. The reference-channel-side is IDM filtered for the connectivity to the total vehicle model. Again, the virtual forces of TB1 are only translational plus one rotation around the Z-axis.

In figure 3.14 the equivalent forces for the two test benches are shown. From these results the following observations can be made:

- **Observation:** All equivalent forces show a declining magnitude over frequency. All forces are in every direction in the same order of magnitude. Intuitively, one could expect a higher force in Y-direction. However, the forces on the tie-rods are quasi-static and not resulting in higher dynamic forces in that direction.
- **Observation:** The translational equivalent forces of VP1 and VP3 are shown in figure 3.14. The four upper graphs show that the forces match very well and the following phenomena can be clearly observed:
 1. The measured interface forces on TB1 dive on three points clearly below the forces determined with the *in-situ* method. On VP1 in the X-direction, the first dip around 1100 Hz is caused by the first (bending) mode, the second one around 3600 Hz is due to the rotational mode around the Z-axis. The last dip is explained by the fact that the rigid assumption does not hold for these high frequencies. The effect is even more clearly observed in the forces on VP3 in Y-direction. It is possible to compensate for this non-rigidity of the test bench, using the receptance matrix \mathbf{Y}_{22}^A of the steering gear and the operational displacements of the interface. This *non-rigid test bench compensation* (NRTB) (equation (1.18)) has been studied, but not shown here for the reason that the \mathbf{Y}_{22}^A model is poor and only available in the band of 0-3200 Hz resulting in an over-estimation of the compensation for the non-rigidity.
 2. The equivalent forces in Z-direction of TB1 show up to 3500 Hz significantly higher force magnitude than the direct force measurement on TB1 and the *in-situ* method. This over-estimation of the forces is due to the bad determination of the dynamics of the support in Z-direction i.e. in that direction the support is very stiff. Combined with the bad signal-to-noise ratio of the operational excitations in that direction, see figure 3.13, the measurement errors are amplified.
 3. The equivalent forces on both test benches degrade in quality above 4000 Hz, which is due to dropping hammer consistency due to presumably decreasing input

APS, see appendix D.1. For TB1 the hammer consistency drops more than for TB2. Together with the dropping signal-to-noise ratio, the uncertainty of the correctness of the equivalent forces is increasing.

- **Observation:** Rotational equivalent forces are approximately 2 orders lower than the translational forces, the contribution to the prediction will be discussed in the next section. The virtual forces match well, for virtual point VP3 up to 3500 Hz and on VP2 even up to 4500 Hz. On all 4 virtual points of TB1 the rotational forces increase significantly, which is not explained easily but are a combination of signal-to-noise and consistency issues.

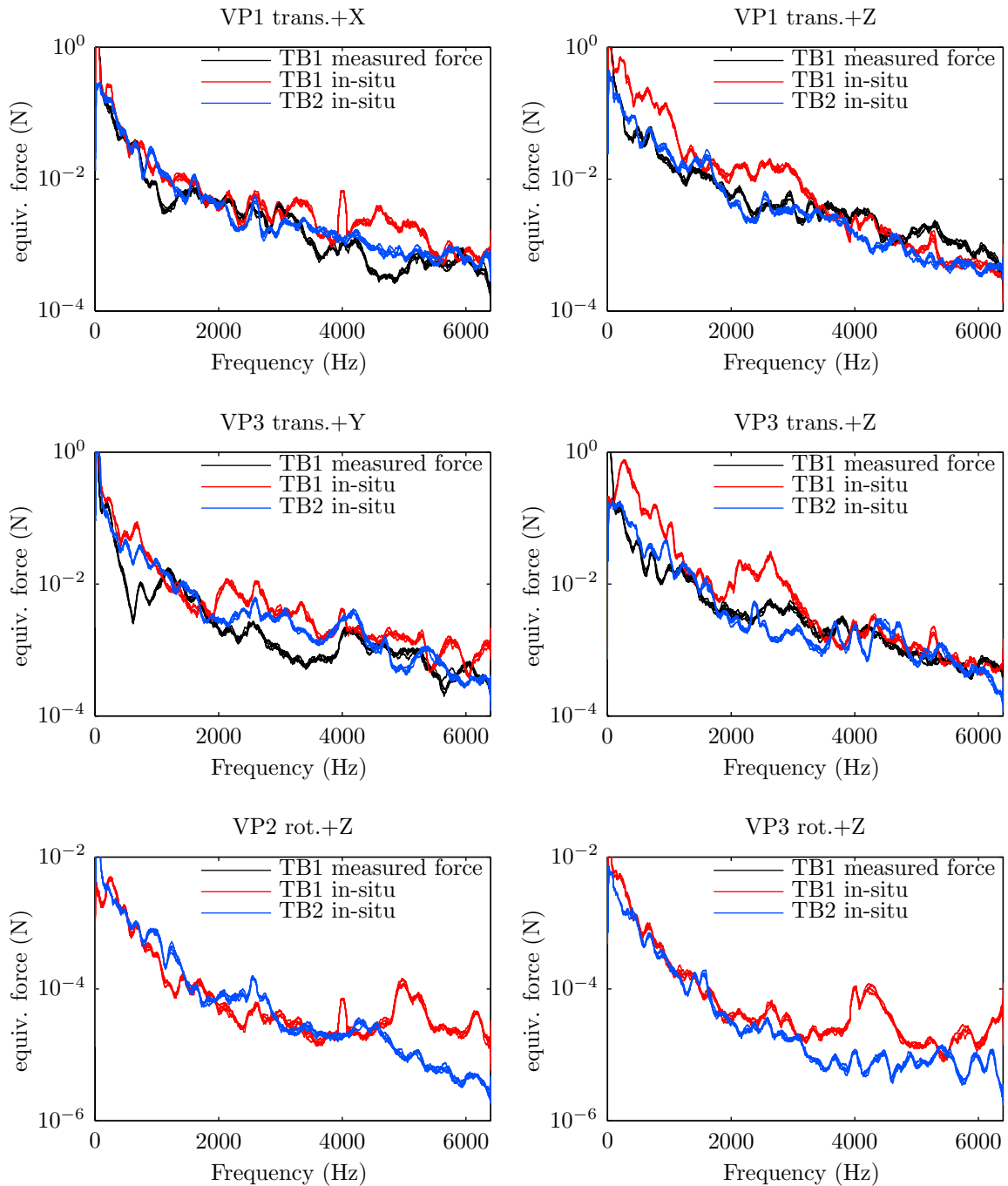


Figure 3.14: The equivalent forces on both test benches determined with direct force measurement and the in-situ method.

3.6.7 Noise prediction

The Component TPA Method for the steering gear in the vehicle with the use of different equivalent force determination schemes is validated in this section. The sound pressure at the driver's ear is determined by use of the measurement results from the sections above. As the *in-situ* method on the TB2 - steering gear shows more reliable equivalent forces than the TB1 - steering gear measurements, these will be used for the synthesis. An additional motivation to use these measurements, is that these f^{eq} are described with 6 DoFs.

The synthesis is made in three steps:

1. **Direct force application:** The measured equivalent forces at the interface of the steering gear and the test bench TB1 are applied directly to determine the sound pressure at the driver's ear;
2. **Synthesis with in-situ method:** The equivalent forces determined on test bench TB2 with the *in-situ* method are used for the prediction of the sound pressure.

The prediction itself comprises a multiplication of the equivalent forces to the mechanical-acoustic total vehicle FRFs from the interface to the reference channel according to equation (1.8). Despite of the fact that the validation measurements in 3.6.1 have shown that they are dominated by the noise of the steering robot, the synthesised response is compared to the validation measurement. This can be justified by the fact that the calculated response, should *not* exceed this noise level, otherwise the response is over-estimated.

In figure 3.15 the calculated prediction at the outer and inner driver's ear is shown. In the upper two graphs the acoustic pressure is calculated with the equivalent forces of both test benches. In the lower graphs, the translational and rotational contributions of the equivalent forces determined in the 6 DoFs description of TB2. Acoustic (sound) pressure is not one-to-one perceived by the human ear as measured by a microphone. One could say that the three bones in the middle ear act as a mechanical filter of sound. The human receptance of loudness is non-linearly dependent over the frequency. On average, the absolute threshold of hearing (ATH) is 20 μPa at 1000 Hz for a young human with undamaged hearing. One method to relate acoustic pressure to perceived sound is to apply A-weighting, in which the ATH is equal to 0 dB. In figure 3.16 the A-weighted sound pressure level is shown.

Some noteworthy observations:

- **Observation:** The synthesised acoustic pressures following from the 2 different equivalent force determination schemes *and* of the two different test benches are remarkably similar, even for high frequencies. This result shows that the equivalent forces determined on both test benches, are independent from the test-bench.
- **Observation:** In this particular practical example, measured translational forces are sufficient to predict the noise level at the driver's ear. Keeping the magnitudes of the mechanical-acoustical FRFs from figure 3.8 and the magnitude of the rotational equivalent forces from figure 3.14 in mind, this is easily explained. The magnitude rotational total vehicle FRFs are 1 order higher than the translational FRFs, but the rotational f^{eq} are 2 orders lower in magnitude in comparison with translational forces, resulting limited contribution of rotational information.

- **Observation:** When synthesising a response with the use of a more compliant test bench like TB2, rotational DoFs are necessary to build a trustworthy response. In the two lower graphs of figure 3.15 it is observed that the rotational DoFs have a small contribution to the acoustic pressure at the driver's ear under 4000 Hz. In the upper part of the band (>4000 Hz) the contribution is equal in terms of magnitude. However, it has to be kept in mind that the signal-to-noise ratio for these high frequencies is limited.
- **Observation:** In figure 3.16 it can be seen that up to 500 Hz the response determined with *in-situ* method are higher than the directly measured forces. Over-estimation of the response in the low frequency band has been observed in earlier studies with model-based equivalent force determination [35]. Around 300 Hz the responses of both methods are equal. As in figure F.3 can be seen, the dynamic stiffness is low due to an eigenfrequency, which results in a good SNR.
- **Observation:** The dips observed in the (measured) equivalent forces of TB1 (see section 3.6.6) have not propagated in a clear difference in response. This can be explained by the dip around 600 Hz in the mechanic-acoustic FRFs shown in figure 3.8.
- **Observation:** The overall sound level of the steering gear to the vehicle's interior noise is very small, as can be seen in figure 3.16. This is verified by performing a steering-by-hand noise measurement, where only some low frequent noise is observed.

3.7 Summary

The theory depicted in part I is applied to the steering gear in a BMW 5-series vehicle. Chapter 3 kicks off with a detailed description of all structures involved in the analysis. Together with the operational conditions a validation strategy is enrolled to predict the noise level in the vehicle with the use of two component TPA methods on two test benches with different structural properties.

It has been shown that the equivalent forces, determined on the test benches with different methods, are remarkably similar. These interface forces yield similar predictions of the sound pressure levels at the driver's ear. As the steering system is actually very quiet, SNR problems let the predicted noise to be compared to the validation measurements.

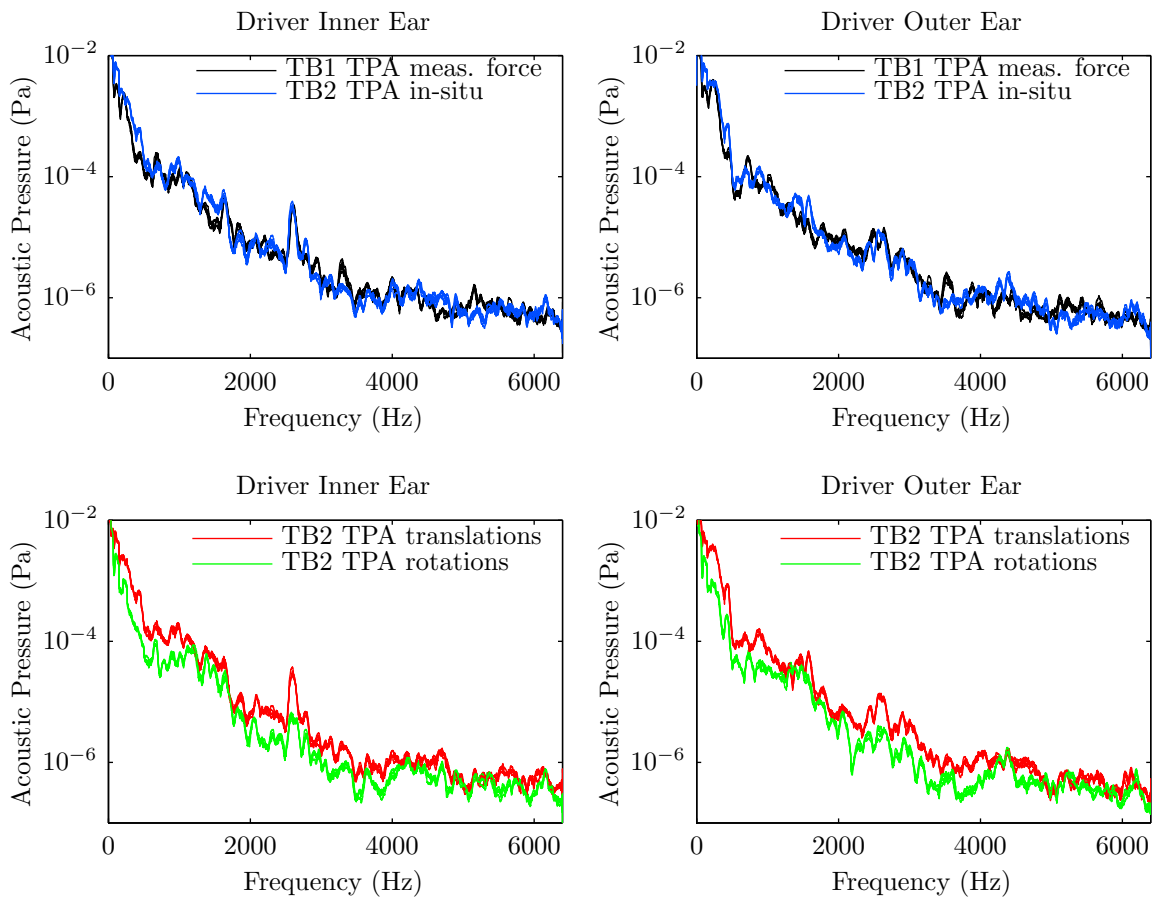


Figure 3.15: The predicted sound pressure at the driver's ear determined with the equivalent forces on TB1 and TB2. In the 2 lower figures, the translational and rotational contributions of the in-situ equivalent forces of TB2 separated.

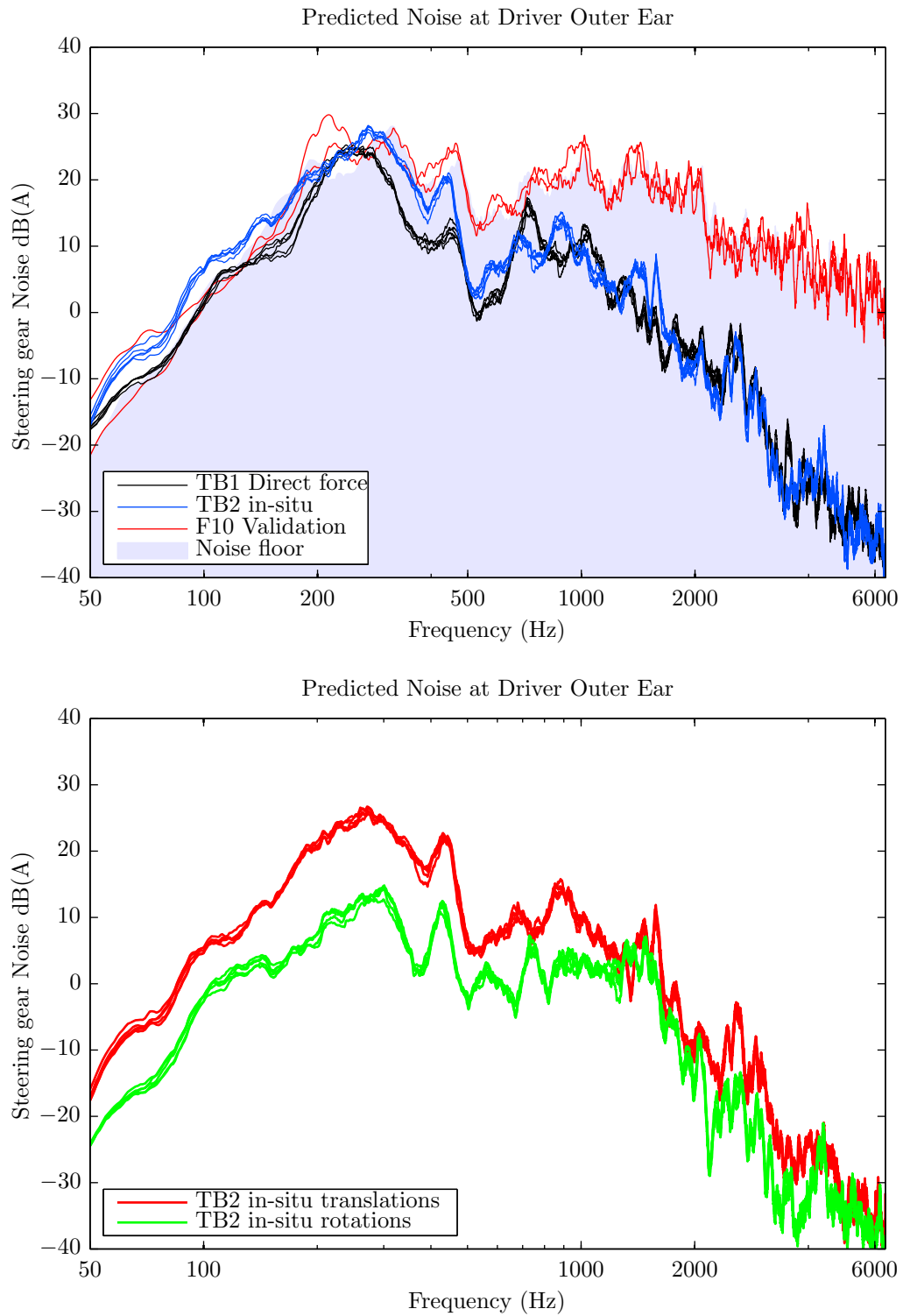


Figure 3.16: The A-weighted predicted sound pressure at the driver's ear for TB2. In the upper graphs the 2 synthesised responses are compared to the validation measurement and the noise from the steering robot. In the lower graph, the translational and rotational contributions of the in-situ equivalent forces of TB2 are separately shown.

Part III

Conclusions and Recommendations

Conclusions

In this thesis, a component Transfer Path Analysis (TPA) is performed to determine the mechanical vibration propagation of a steering gear to the driver's ear in the vehicle in a multi-kHz range. The component TPA methodology is presented in the frequency domain according to the Dynamic Substructuring (DS) approach for the identification of the internal component excitations on a test bench. The internal excitation forces are characterised as a set of equivalent forces determined from interface force and acceleration measurements at the interface of the active/source component and a test bench. This is valid under the condition that the internal excitation forces in the steering gear in the vehicle are equal to internal excitation force of the steering gear on the test bench i.e. the excitations are *independent* of the dynamic response and deformation of the steering gear.

Various methods for the equivalent force determination have been presented which yield theoretically to the same - test bench independent - set of forces. The response is synthesised by a multiplication of the equivalent forces with the Frequency Response Functions (FRFs) of the total system from the interface to the point of interest on the corresponding interface Degrees of Freedom (DoFs).

The validation of the independence of the equivalent forces has been performed with two equivalent force determination schemes applied to a steering gear on two test benches with different stiffness properties. The two characterized equivalent force determination methods, are the *in-situ* force determination scheme and the directly measured interface forces. Both schemes show generally equal spectra over the entire frequency band.

The direct interface equivalent forces show that the dynamic properties influence the force determination. As expected, the equivalent forces are under-estimated in the vicinity the the resonant frequencies of the test bench.

The equivalent forces determined with the *in-situ* method show that they are dependent on the quality of the dynamic model of the assembly. In the lower frequency band a low signal-to-noise ratio yields an over-estimated equivalent force caused by the inverse nature of the technique. In the upper frequency band the quality of the dynamic model suffers from a low input Auto Power Spectrum (APS) for the determination of the FRFs.

Furthermore, it has been validated that unmeasurable rotational forces can be determined and are required to synthesise the response with the model-based *in-situ* equivalent force determination scheme.

The method used to experimentally determine unmeasurable rotational DoFs for the connectivity of the substructures, is the virtual point transformation. The projection of measured Frequency Response Functions (FRFs) on local rigid Interface Displacement Modes (IMDs) reduces the influence of noise and calculates the dynamics in a user specified virtual point. The method has been validated by modelling an interface point of a steering gear and a vehicle on three separate vehicles. The determination of the interface FRFs are enhanced by a sufficient over-determined reduction step in terms of noise- suppression and mode observability. In the low frequency band, where the response of systems is usually low, FRFs with overshoots and bias errors dominate the transformation caused by the Least-Squares approximation in the interface reduction step. In the high-frequency region, a degrading virtual point transformation

is mainly caused by a decreasing impulse excitation APS. Stronger impact excitations improve the impact spectrum but enlarge the risk of e.g. output-signal problems.

It has been shown that using a structured procedure for the virtual point transformation by pre-analyses on the reduction step and the use of quality indicators, the model can be determined with confidence. Furthermore, it has been showed that by the use of modal fitting techniques low frequent distortions of FRFs can be repaired to enhance the virtual point transformation.

Recommendations

Throughout this thesis, a number of aspects have been observed that could improve the results for the equivalent-force TPA and the connectivity of substructures. These challenges lead to the following recommendations for future research:

- **Apply methodology on an academic case**

In the thesis, the different equivalent force determination schemes are applied on two test benches with different tie-rod force generation. It is recommended to perform measurements on an identical test bench, but with different supports. In this way, unknown test-bench dependent influences are minimised and one could focus more on the application of the methodology under equal conditions. Furthermore, it is recommended to improve the decoupling of surrounding, noise inducing systems.

One could go even further and apply the methodology on a more academic case to qualify the various force determination schemes. A less complex structure with only one or two interface points and a vibration source with steady state excitations e.g. an electric actuator with an unbalanced rotor. Furthermore, a point of interest could be chosen such that a validation measurement is easier to obtain and with a significant signal-to-noise ratio.

- **Towards 'live Virtual Point transformation'**

The sensor and impact excitation positions and orientations throughout this work have been predefined. The spatial transformation of FRFs on the Interface Displacement Modes (IDMs) is pre-analysed to check if the virtual point DoFs (both forces and accelerations) are well observable. As the quality of the impact excitations are dependent on the skills of the user, measurement errors are easily made. This especially goes up for impact positions with a 'small arm' with respect to the virtual point and wrong moment-excitations are easily produced. Therefore, it would be advantageous for the transformation to develop impact position/orientation detection systems. These systems will as-well take away the need for a pre-evaluation of the transformation as this can be done 'on-the-fly'.

- **Study the construction of the interface reduction transformation matrix**

The interface reduction step for the calculation of the virtual point degrees of freedom, is performed with a least-squares approximation. Due to this approach, the physical background is often lost e.g. it is observed that (reference) channels end up in virtual point DoFs but they are physically orthogonal to on-another. One could get more grip

on the construction of the transformation matrix \mathbf{T} through either a weighting matrix or the development of an alternative method for an improved virtual point transformation with a more physical background.

- **Validity rigid IDMs**

Determine the minimal percentage of impact/sensor consistency necessary for a successful determination of the interface DoFs for coupling procedures. Hereafter the considered frequency band can possibly be extended by the use of flexible interface modes as long as the can be defined equally for both the active and the receiving structure.

- **Improve FRF measurements**

The balance between the amount of force required for the excitation of all the modes within the considered frequency bandwidth and the saturation of the sensor is challenging, especially impacts in the vicinity of the sensors. The force input spectrum has a large share in the quality of the virtual point transformed FRFs and has to be monitored well. Therefore, it is recommended to avoid for impacts close to the sensor and monitor the input spectrum. A pre-analysis on the choice of sensors/impact hammer combination with respect to the considered frequency band is important.

One can also think of alternative measurement techniques like non-contact vibration techniques e.g. laser Doppler vibrometers, but the optical engineering field is unknown to the author.

Appendix A

Frequency Response Function

A Frequency Response Functions (FRFs) represents a frequency dependent complex-valued quantity relating the output and input Degrees of Freedom (DoFs) of a system. In structural dynamics this means the motion $u(\omega)$ related to a force excitation $f(\omega)$ through the complex function with magnitude $|Y(\omega)|$ and phase $\angle Y(\omega)$.

In this appendix the theoretical derivation of a FRF is presented by means of the Equations of Motion (EoM) of a linear, time invariant system. In table A.1 an overview is given of various types of FRFs.

The EoM of discretised mechanical system (or a discrete model) in the time domain is written [10]:

$$\mathbf{M}\ddot{\mathbf{u}}(t) + \mathbf{C}\dot{\mathbf{u}}(t) + \mathbf{K}\mathbf{u}(t) = \mathbf{f}(t) \quad (\text{A.1})$$

The implicit assumption of the system in the equation above is that it is *linear* (the \mathbf{M} , \mathbf{C} and \mathbf{K} matrices are independent on the states of the system) and that it is *time-invariant* (i.e. constant parameters.)

Where \mathbf{M} , \mathbf{C} , \mathbf{K} denote the mass, damping and stiffness matrices respectively of the system, $\mathbf{u}(t)$ represents the vector of degrees of freedom (DoFs) and $\mathbf{f}(t)$ denotes the externally applied forces on the DoFs of the system. In the thesis, extensive use is made of subsystem matrices, e.g. the mass matrix and displacement vector are defined as:

$$\mathbf{M} = \begin{bmatrix} \mathbf{M}_{11} & \dots & \mathbf{M}_{1j} \\ \vdots & \ddots & \vdots \\ \mathbf{M}_{i1} & \dots & \mathbf{M}_{ij} \end{bmatrix}, \quad \mathbf{u} = \begin{bmatrix} \mathbf{u}_1 \\ \vdots \\ \mathbf{u}_i \end{bmatrix}, \quad \mathbf{f} = \begin{bmatrix} \mathbf{f}_1 \\ \vdots \\ \mathbf{f}_i \end{bmatrix} \quad (\text{A.2})$$

where the subscript l denotes the number of displacement DoF and k the number of force DoF. Note that the matrix partitions, e.g. \mathbf{M}_{kl} , itself can include multiple degrees of freedom as-well. It is not a necessary condition for the system of equations in (A.1) to be independent on the states and invariant in time to get a solution. Non-linear systems can be solved too using time integration schemes and iterative solvers, but that is not in the interest in this thesis.

	Response/Force		Force/Response	
$\mathbf{u}(\omega)$	Receptance	\mathbf{Y}	Dynamic Stiffness	\mathbf{Z}
$\dot{\mathbf{u}}(\omega)$	Admittance/ Mobility	$\mathbf{Y}_{mob.} = j\omega\mathbf{Y}$	Mechanical Impedance	$\mathbf{Z}_{m.imp} = \frac{1}{i\omega}\mathbf{Z}$
$\ddot{\mathbf{u}}(\omega)$	Accelerance/ Inertance	$\mathbf{Y}_{acc.} = -\omega^2\mathbf{Y}$	Dynamic Mass	$\mathbf{Z}_{m.mass} = \frac{1}{-\omega^2}\mathbf{Z}$

Table A.1: Types of frequency response functions for a force impact (N).

The *steady-state* assumption for the EoM Transformation from the time-domain to the frequency-domain of a signal $x(t)$ via the Fourier transformation:

$$x(j\omega) = \mathcal{F}_t[x(t)] = \int_{-\infty}^{\infty} x(t) e^{-j\omega t} dt \quad (\text{A.3})$$

The time functions of the displacement, velocity and acceleration vectors in equation (A.1), hence $\mathbf{u}(t)$, $\dot{\mathbf{u}}(t)$ and $\ddot{\mathbf{u}}(t)$, can thus be transformed to the frequency domain with equation (A.3). For the time derivatives, with the order indicated with n , of the displacements, the fact that the motion is bounded in time due to damping in a system, the transformation yields:

$$(j\omega)^n \mathbf{u}(j\omega) = \int_{-\infty}^{\infty} \frac{d^n \mathbf{u}(t)}{dt^n} e^{-j\omega t} dt \quad (\text{A.4})$$

Which yields for the EoM in equation (A.1):

$$\left(-\omega^2 \mathbf{M} - j\omega \mathbf{C} + \mathbf{K}\right) \mathbf{u}(j\omega) = \mathbf{f}(j\omega) \quad (\text{A.5})$$

Now the *dynamic stiffness* and *receptance* matrices can be defined (omitting explicit dependency on frequency):

$$\mathbf{Z} \triangleq -\omega^2 \mathbf{M} - j\omega \mathbf{C} + \mathbf{K} \quad (\text{A.6})$$

$$\mathbf{Y} \triangleq \mathbf{Z}^{-1} \quad (\text{A.7})$$

The receptance matrix \mathbf{Y} , is preferred in experimental dynamic analyses as usually accelerations are measured in response to a force excitation. For the sake of completion, the most common dynamic stiffnesses and receptances are shown in table A.1. These quantities are related to each other by differentiation and integration in the time-domain, which means a multiplication/division with the complex frequency ($j\omega$) in the frequency domain.

Appendix B

Dynamic Substructuring

The concept of Dynamic Substructuring (DS) is to divide large and/or complex structures in to smaller so-called substructures. There has been a lot of interest shown in substructure coupling and de-coupling techniques, especially in the context of experimental applications [11, 21, 25, 37, 40, 41]. There is a lot of research done on a number of remaining challenges in the practical and robust implementation of DS e.g. interface effects and error propagation of measurement errors [7, 33, 40].

Lagrange Multiplier Frequency Based Substructuring

The equations of motion of n unassembled subsystems in blockdiagonal format in the frequency domain can be written as:

$$\mathbf{Z}(\omega)\mathbf{u}(\omega) = \mathbf{f}(\omega) + \mathbf{g}(\omega) \quad (\text{B.1})$$

with the dynamic stiffness matrix \mathbf{Z} of the assembled structure, the sets of displacements \mathbf{u} , external forces \mathbf{f} and interface forces \mathbf{g} are defined as ¹

$$\mathbf{Z} \triangleq \text{diag}(\mathbf{Z}^{(1)}, \dots, \mathbf{Z}^{(n)}), \quad \mathbf{u} \triangleq \begin{bmatrix} \mathbf{u}^{(1)} \\ \vdots \\ \mathbf{u}^{(n)} \end{bmatrix}, \quad \mathbf{f} \triangleq \begin{bmatrix} \mathbf{f}^{(1)} \\ \vdots \\ \mathbf{f}^{(n)} \end{bmatrix}, \quad \mathbf{g} \triangleq \begin{bmatrix} \mathbf{g}^{(1)} \\ \vdots \\ \mathbf{g}^{(n)} \end{bmatrix}$$

Suppose the interface degrees of freedom $u^{(l)}$ and $u^{(k)}$ of a coinciding interface node of n rigidly connected substructures. Two conditions are to be satisfied for coupling, hence:

1. *Compatibility*: the coupled DoFs do not undergo relative displacement to one another i.e. $u^{(l)} - u^{(k)} = 0$. The compatibility condition can be expressed by

$$\mathbf{B}\mathbf{u} = \mathbf{0} \quad (\text{B.2})$$

¹see appendix A for the definition of the dynamic stiffness matrix. The explicit notation of the dependence on frequency (ω) is omitted.

The matrix \mathbf{B} operates on the interface degrees of freedom and is a signed Boolean matrix if the nodes are spatially matching.

2. *Equilibrium*: when summing the dual connection forces, the resultant has to be zero i.e. $g^{(l)} + g^{(k)} = 0$. Then equilibrium condition is expressed by

$$\mathbf{L}^T \mathbf{g} = \mathbf{0} \quad (\text{B.3})$$

The matrix \mathbf{L} is the Boolean matrix localising the interface DoFs from the global dual set of DoFs. For more details on both the matrices \mathbf{B} and \mathbf{L} , see [25].

Multiple coupling techniques for discretised domains exist, which can be applied to either the physical, frequency or modal domain. In this appendix, the dual assembly approach is covered. In this formulation the full set of global DoFs is retained. The dual assembled structure is obtained by *a priori* satisfying the interface equilibrium condition. For more details on both approaches, the reader is referred to [25].

In the dual assembly approach, the connection forces are described by Lagrange multipliers. The equilibrium condition is satisfied by

$$\mathbf{g} = -\mathbf{B}^T \boldsymbol{\lambda}$$

where $\boldsymbol{\lambda}$ represents the set of Lagrange multipliers which are interface force intensities acting on the corresponding interface degree of freedom. Due to the construction of Boolean matrix \mathbf{B} , the interface forces are equal and in opposite direction for all pairs of dual coupling DoFs. The equilibrium condition of equation (B.3) writes

$$\mathbf{L}^T \mathbf{g} = -\mathbf{L}^T \mathbf{B}^T \boldsymbol{\lambda} = \mathbf{0}$$

It can be shown that \mathbf{L}^T is the nullspace of \mathbf{B}^T . Thus satisfying conditions (B.2) and (B.3) the system of equations in (B.1) writes

$$\begin{bmatrix} \mathbf{Z} & \mathbf{B}^T \\ \mathbf{B} & \mathbf{0} \end{bmatrix} \begin{bmatrix} \mathbf{u} \\ \boldsymbol{\lambda} \end{bmatrix} = \begin{bmatrix} \mathbf{f} \\ \mathbf{0} \end{bmatrix} \quad (\text{B.4})$$

This system of equations can be easily solved when the dynamic stiffness \mathbf{Z} is available. However, in experimental dynamics one measures the receptance matrix \mathbf{Y} of the (sub)systems. As this matrix is the inverse of the dynamic stiffness matrix, the system of equations in (B.4) is not directly solved. Eliminating the Lagrange multipliers, the dual interface problem in the frequency domain, suitable for coupling of receptance matrices is obtained

$$\mathbf{u} = \mathbf{Y} \mathbf{f} - \mathbf{Y} \mathbf{B}^T (\mathbf{B} \mathbf{Y} \mathbf{B}^T)^{-1} \mathbf{B} \mathbf{Y} \mathbf{f} \quad (\text{B.5})$$

Appendix C

Experimental Modal Analysis

In modal analysis a structure is evaluated on its dynamic properties and described by its natural characteristics: *eigen frequency*, *damping* and *mode shapes*. With these *modal* parameters it is attempted to build a model of the structural dynamic behaviour.

In Experimental Modal Analysis (EMA) the modal parameters are extracted from experimentally obtained data with distinct transducers applied to the structure. Hereafter, a identification method is used to build a mathematical model with the modal parameters. In this appendix a pole/residue model is derived, where-after a modal parameters estimation technique based on that model is discussed.

Pole/Residue Model

The Pole/Residue parametrisation is one of such a single and multi degree of freedom identification methods. This model considers poles and residues as unknowns to describe the Frequency Response Functions (FRFs). These variables are closely related to the modal parameters. Applying the Fourier transformation to a one degree of freedom according to the Equations of Motion (EoM) of a mechanical system described in equation (A.1), one can write the system transfer function via the polynomial form in the partial fraction expansion form:

$$Y(\omega) = \frac{1}{-\omega^2 m + (j\omega)c + k}$$
$$Y(\omega) = \frac{1/m}{(j\omega - \lambda)(j\omega - \bar{\lambda})} = \frac{R}{j\omega - \lambda} + \frac{\bar{R}}{j\omega - \bar{\lambda}} \quad (\text{C.1})$$

Here denote R and \bar{R} the residues of the transfer function and λ and $\bar{\lambda}$ the complex conjugate poles which follow from the characteristic equation in the denominator of the transfer function:

$$\lambda_{1,2} = -\frac{c}{2m} \pm \sqrt{\left(\frac{c}{2m}\right)^2 + \frac{k}{m}} = -\zeta\omega_n \pm \sqrt{(\zeta\omega_n)^2 - (\omega_n)^2} = -\sigma \pm j\omega_d$$

where

ω_n	$= \sqrt{k/m}$	Natural frequency (rad/s)
ζ	$= c/(2m\omega_n)$	Damping ratio (-)
ω_d	$= \omega_n\sqrt{1-\zeta^2}$	Damped natural frequency (rad/s)
σ	$= \zeta\omega_n$	Damping factor *-(-)

The result above can be extended for a multi degree of freedom (MDoF) system of order $2N$ by summing up all contributions of the modes k according to the superposition principle. The eigen-values and corresponding modes come in complex conjugate pairs for structures with subcritically damped modes [10, 15] and therefore the system is written as

$$\mathbf{Y}(\omega) = \sum_{k=1}^N \frac{\mathbf{R}_k}{j\omega - \lambda_k} + \frac{\overline{\mathbf{R}}_k}{j\omega - \overline{\lambda}_k} \quad (\text{C.2})$$

The residue matrix \mathbf{R}_k is of rank one, and can therefore be decomposed as:

$$\mathbf{R}_k = Q_k \phi_k \phi_k^T \quad (\text{C.3})$$

where ϕ_k is the modeshape and Q_k is a scaling factor for mode k depending on how ϕ_k are normalised. Possible scaling factors for Q_k are:

- Unity modal mass: $Q_k = \frac{1}{2j\omega_k}$;
- Unity scaling factor: $Q_k = \mathbf{R}_k (\phi_k \phi_k^T)^{-1} = 1$.

The residue matrix for mode k is built by the multiplication of the mode shape with its own transpose i.e. the outer product as can be seen in equation (C.3). Therefore, every *row and column* contain the mode, multiplied with a different shape component.

For the extraction of the mode shape, it is required to perform a driving point measurement or a triangular measurement [34].

Modal Identification methods

In order to fit transfer function measurements to a modal parametric model, the modal parameters have to be obtained. Numerous modal parameter estimation methods exist and can be classified as follows

Time- vs. frequency domain methods

The estimation of the modal parameters can be performed in either the time domain with the time domain with e.g. the Least-Squares Complex Exponential method [34] or the frequency domain model in (C.2), which will be used in this thesis.

SDoF vs. MDoF methods

Single DoF methods are used on lightly damped systems with well separated eigenfrequencies in the considered frequency band. For example *peak picking* and *circle fit* methods are used in SDoF modal identification methods [4]. MDoF models are used on systems with more heavily damped and closely spaced modes in the considered frequency band. An example is the pole/residue model identification method of Balmès [6], which is explored here.

Local vs. global estimation methods

Local estimation methods extract the modal parameters of each individual FRF in a measured set. To describe a full system it has to be decided by the user which poles have to be used. However, locally estimated poles can influence the fit of the residues when finding the global dynamics. Global parameter estimation methods attempt to extract the system poles which describe all frequency response functions in a minimum sense. These system poles are hereafter used to fit the residues to the measured transfer functions.

The choice for a particular method is driven by the the natural characteristics of the structure but it is up to the user to judge the validity of a synthesised FRF.

In practice, the structure is only measured in a limited frequency band. As real structures have an infinite number of poles the mathematical model in equation (C.2) is extended to include the out-of-band residual effect with additional terms to approximate these modes [6]:

$$\mathbf{Y}(\omega) = \sum_{k=1}^N \left(\frac{\mathbf{R}_k}{j\omega - \lambda_k} + \frac{\bar{\mathbf{R}}_k}{j\omega - \bar{\lambda}_k} \right) - \frac{\mathbf{F}}{\omega^2} + \mathbf{E} \quad (\text{C.4})$$

where the residual mass term \mathbf{F} is used to approximate the modes below the lower bound ω_{min} of the frequency band and the residual stiffness term \mathbf{E} approximates the modes above the upper frequency bound ω_{max} . The residual terms can have a significant influence on the model and therefore, one has to know what terms to take into account to properly approximate the FRF.

The MDoF modal parameter estimation method by Balmès [6] uses the model in equation (C.4). In order to find an approximation of the model to the a measured set of FRFs, a two step optimisation scheme is used. The poles are considered as unknowns and the residues as implicit functions of the poles. Therefore, the model can be rewritten in matrix form as:

$$\mathbf{Y}(\lambda_k, \mathbf{R}, \omega) = \Phi(\lambda_k, \omega) \mathbf{R}(\lambda_k) \quad (\text{C.5})$$

where $\mathbf{R}(\lambda)_k = [\mathbf{R}, \mathbf{F}, \mathbf{E}]$ contains the residues and the residual terms and the matrix $\Phi(\lambda_k, \omega)$ contains the temporal part of the FRFs i.e. the denominator of (C.4). Key to successful residue estimation and non-linear pole optimisation is the expansion of the residues into real and imaginary parts i.e. $\mathbf{R}_k = \mathbf{U}_k + j\mathbf{V}_k$. With an initial estimation of the poles¹, the residues are approximated by solving the linear least-squares problem

$$\mathbf{R}(\lambda_k) = \left(\Phi^T(\lambda_k, \omega) \Phi(\lambda_k, \omega) \right)^{-1} \Phi^T(\lambda_k, \omega) \mathbf{Y} \quad (\text{C.6})$$

the residues are substituted into equation (C.5) to build the fitted FRFs \mathbf{Y}_{fit} .

Before improving the initial pole estimations with a non-linear update scheme, it has to be evaluated how well \mathbf{Y} is represented by \mathbf{Y}_{fit} with a cost function J . For example, a quadratic cost function leads to the expression:

$$J = trace \left((\mathbf{Y}_{fit} - \mathbf{Y})^T (\mathbf{Y}_{fit} - \mathbf{Y}) \right) \quad (\text{C.7})$$

In the method of Balmès the cost function J is minimised with an ad-hoc update scheme for the poles whilst evaluating the residues by a least-squares solution at each step of the optimisation i.e. the Non-Linear Least-Squares minimisation. this algorithm uses small steps on the imaginary and real part of the of pole based on the sign of the gradient. Every time the gradient changes sign, which indicates the passing over the optimum, the step-size is reduced. The error gradient with respect to the real or imaginary part (θ) is defined as:

$$\frac{\partial J}{\partial \theta} = 2(\mathbf{Y}_{fit} - \mathbf{Y})^T \frac{\partial \Phi}{\partial \theta} \mathbf{R} \quad (\text{C.8})$$

This optimisation scheme continues until the evaluated cost function is below a set tolerance, the step-size for the real or imaginary pole parts have been set to zero or a maximum number of iterations is reached. It has been shown that the error gradient with respect to one of the pole locations is almost independent from the error on the other poles, even when very closed spaced modes are present in the system. This makes simultaneous update on the poles very efficient. This ad-hoc scheme does not guarantee convergence as e.g. non-existing or computational poles are non-converging. Extension of the algorithm with constraints on e.g. minimality, reciprocity, properness or proportional has been done in the algorithms of commercial package SDTools[®] and is not covered in this thesis.

¹Visual pole picking, a circle fit method or by CMIF (E)

Appendix D

Experimental FRF Determination

For the experimental approach for the modelling of dynamic behaviour of structures, or modal testing, relies of the extraction of the structural characteristics from measurements. Especially for complex structures, experimental modal testing techniques are considered to be more reliable than numerical approaches e.g. Finite Element models as these rely on assumptions of the structure. In this thesis the experimental modal techniques are applied for applications in the frequency domain, i.e. Frequency Response Function measurements. Structural modal testing in the frequency domain are based on two major assumptions: the structure is linear and the system is stationary as schematically drawn in figure D.1.

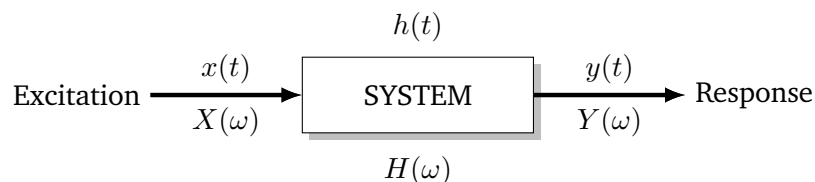


Figure D.1: *The response to an excitation through the linear transfer function in both the time- and frequency domain.*

The topics covered in this appendix are mainly focussed on FRF measurements, however some concepts cover other applications as well. In general the measurement procedure consists out of three steps:

1. Measure the response of a structure to an excitation;
2. Process the acquired data;
3. Analyse the the processed data.

In all three stages of the measurement procedures limitations are present and errors can occur due to e.g. to nature of the structure, measurement equipment, the processing of the data and the skills of the researcher.

In this appendix the signal processing of the measured signals is covered and how FRFs are calculated. Hereafter some practical considerations are discussed on obtaining trustworthy FRFs.

Auto Power Spectrum (APS)

Consider a measured time signal of a quantity $\mathbf{x}_m(t)$ or $\mathbf{y}_m(t)$. Through the Fourier transformation of the auto-correlation function, The Auto Power Spectrum (APS) gives an indication how the mean power of that signal is distributed over frequency

$$\mathbf{G}_{xx}(\omega) = \sum_{m=1}^M \mathbf{X}_m(\omega) \overline{\mathbf{X}_m(\omega)} \quad (\text{D.1})$$

where $\mathbf{X}_m(\omega)$ and the complex conjugated $\overline{\mathbf{X}_m(\omega)}$ denote the Fourier Transform of the measured time signal $\mathbf{x}_m(t)$. This real valued quantity has no information on the phase due to the quadratic nature of the function. The measured quantity together with noise are present in the APS. A practical application of the input APS is to judge whether an impact excitation $\mathbf{x}_m(t)$ has enough energy over the considered frequency band.

Cross Power Spectrum (CPS)

Mutually to the APS, the Cross Power Spectrum (CPS) indicates the mutual power between the spectra of two signals in the considered frequency band

$$\mathbf{G}_{yx}(\omega) = \sum_{m=1}^M \mathbf{Y}_m(\omega) \overline{\mathbf{X}_m(\omega)} \quad (\text{D.2})$$

where $\mathbf{Y}_m(\omega)$ denotes the Fourier Transform of the measured time signal $\mathbf{y}_m(t)$ and $\overline{\mathbf{X}_m(\omega)}$ is the complex conjugate of the measured input spectrum. In contrary to the APS, the CPS contains information about the magnitude and the relative phase of the two considered spectra.

Frequency Response Function estimation

A FRF represents the relationship between the excitation and response signals in the frequency domain. In experimental modal analysis multiple FRF estimators are present of which two will be covered here i.e. the H_1 and H_2 estimators [15]. Both estimators are based on the auto and cross power spectra described in the above. Mathematically both estimators are similar, but both have different properties, which will be shortly covered.

The H_1 -estimator of the transfer function is given by

$$\mathbf{H}_1(\omega) = \frac{\mathbf{G}_{yx}(\omega)}{\mathbf{G}_{xx}(\omega)} \quad (\text{D.3})$$

This transfer function estimator is susceptible to noise on the input of the of the system. Therefore, when noise is present the H_1 -estimator tends to *under*-estimate the actual transfer function of the system as the noise on the output is minimized.

The H_2 estimator of the transfer function is given by

$$\mathbf{H}_2(\omega) = \frac{\mathbf{G}_{yy}(\omega)}{\mathbf{G}_{xy}(\omega)} \quad (\text{D.4})$$

This transfer function estimator is susceptible to noise on the output of the of the system. In the presence noise the H_2 -estimator tends to *over*-estimate the actual transfer function of the system.

D.1 Practical Considerations

As seen in the above, multiple estimation methods exist to calculate a transfer function. In practice, one determines the FRF by measuring the a response to a force excitation, see table A.1. For the force excitation, various signals exist e.g. sine sweeps, random noise and impulse excitation. All excitation techniques have their advantages and weaknesses. As all FRF measurements in this thesis are obtained by the use impact force excitation, the other techniques will not be covered here.

Impact excitation for FRF determination requires knowledge of signal processing and correct settings for signal conditioning and computations¹. Consider a force excitation Dirac-Delta-function according to

$$\delta_a(x) = \frac{1}{a\sqrt{\pi}}e^{-x^2/a^2}$$

A perfect impulse excitation i.e. $a \rightarrow 0$ yields to a uniform APS over an infinite frequency band in the frequency domain. This will result in an excitation of all modes with equal energy. However, practically this can never be realised with an impact hammer operated by a user, which results in a decreasing APS, as illustrated in figure D.2. The following list has to be considered while measuring

Hammer specifications The force spectrum can be influenced by the material selection of the hammer tip. A hard tip has a short pulse and excites a wider frequency range than a softer tip. The weight of the hammer is of great importance too i.e. heavier hammer yield to higher force impacts more easily. Furthermore, the measurement range and sensitivity of the force transducer in the hammer has to correspond with the amount of force required for the frequency band of interest.

APS The impact excitation has to contain enough energy to excite all modes in the frequency band of interest. An acceptable roll-off of the APS of the hammer is about 15-20 dB [5]. If a rather small frequency band is considered, the impact energy has to be lowered as well to avoid exciting out-of-band modes which distort the measured FRF.

¹Signal conditioning settings e.g. pre-trigger, force windows, exponential output functions, range settings for the response channels etcetera are not discussed here.

Consistent magnitude High impacts can overdrive a structure and induce amplitude dependent dynamics i.e. non-linearities. Local flexibilities have to be considered with respect to the amount of force required for the right input APS. A consistent but high input spectrum imparts possibly energy into the structure beyond the band of interest and may not yield to coherent responses due to saturation or overloads.

Consistent alignment misalignment of impacts, in both position and direction, will effect FRF measurements and the accuracy of reciprocity between the input and output DoFs.

Double impact The input spectrum is heavily distorted over the entire frequency band by double or multiple impacts and should obviously be avoided.

Practice

Consider the two test benches TB1 and TB2 with the steering gear mounted. As both structures have different stiffness properties, different force levels are required to obtain the right input spectrum for the bandwidth under consideration. In figure D.2 some typical force excitation spectra are shown. The following observations can be made

- The magnitude of the input force for a flat input spectrum are quite different for the two test benches. It can be seen that the 1st and 2nd excitation on both structures show a reasonable input spectrum for the force excitation of the structure, within a roll-off of -15 dB.
- The 3rd and 4th excitations on the corresponding structure, show that the impact is not short enough and that the magnitude of the excitation is too low. This results in the 'bouncing' effect caused by the harmonic-like excitation signal.
- The softer impacts show a kind of ripple effect on the APS, which is undesirable.

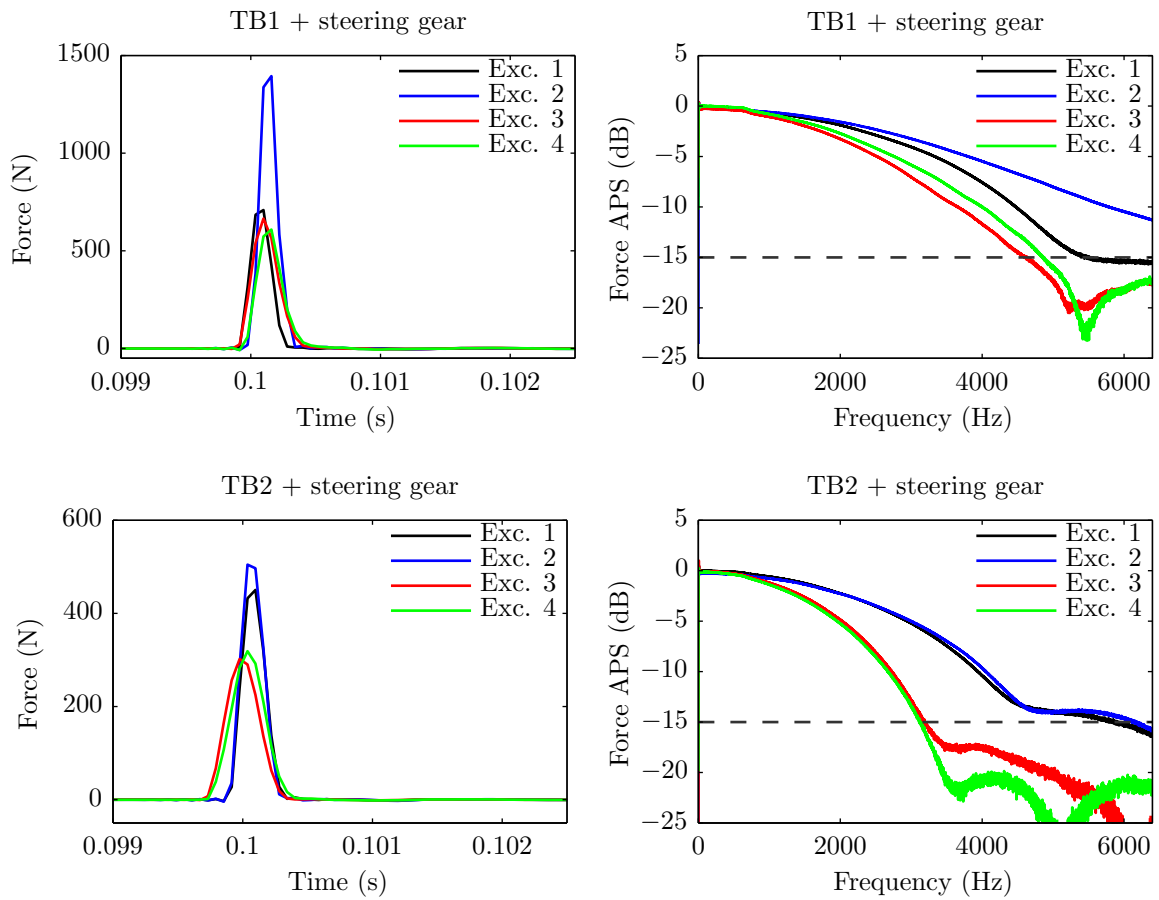


Figure D.2: Impact excitations on both test-benches with the steering gear mounted. In the left figures, the force impact in the time-domain, the right figures show the APS of the impacts.

Appendix E

Complex Mode Indicator Function

Singular Value Decomposition

Singular Value Decomposition (SVD) is a factorisation technique of a real or complex matrix. SVD of any $(n \times m)$ matrix \mathbf{A} has the form:

$$\mathbf{A} = \mathbf{U}\mathbf{\Sigma}\mathbf{V}^T \quad (\text{E.1})$$

where \mathbf{U} is an $n \times n$ orthonormal matrix consisting of the left singular vectors of \mathbf{A} , \mathbf{V} is an $m \times m$ orthonormal matrix whose columns are the right singular vectors of \mathbf{A} . The matrix $\mathbf{\Sigma}$ is of size $n \times m$ with only diagonal elements, the singular values $s_1 \dots s_m$ of \mathbf{A} . SVD is closely related to the eigenvalue decomposition as the singular values are equal to the square root of the eigenvalues λ of the matrix $\mathbf{A}^T \mathbf{A}$. The rank of the matrix \mathbf{A} is equal to the number of positive singular values.

Singular value decomposition can be used for noise reduction while inverting ill-conditioned matrices. After the application of SVD on a matrix, a tolerance can be set on the absolute value of the singular value (e.g. relative to the largest singular value) to reduce the error amplification of measurement errors in a FRF-matrix. These techniques are called singular value rejection methods [39].

CMIF

The Complex Mode Indicator Function (CMIF) is developed to indicate the existence and location of modes as an aid for model order determination and used for the approximation of modal parameters [17]. CMIF is based on SVD of the FRF-matrix. CMIF is used to identify the principal modes observed in the set of measurements within the accuracy of the frequency resolution.

A singular value decomposition is performed at each spectral line of the FRF-matrix. The CMIF is a plot of the log-magnitude of the singular values of the FRF matrix as a function of

frequency. No more modes than the small dimension of the FRF-matrix can be observed. Multiple poles are indicated by multiple significant singular values peaking at the same distinctive frequency. Therefore, one can detect repeated and closely spaced modes. At the resonances, the mode-shapes are represented by the corresponding left singular vector.

As explained, the modes of the system are indicated by the peaks in the CMIF plot, but not every peak indicates a mode. Peaks can as well be created by measurement noise, leakage, non-linearities and the so-called CMIF-crossover effect, which can be observed in the dynamics of TB2 in figure F.5 around the two first close resonance frequencies. The latter is a peak created by the succession of next dominant mode along the frequency axis. This effect can be addressed by mode tracking, which is done by the use of the Modal Assurance Criterion (MAC) [2] of the left singular vector to the preceding vector [1].

Appendix F

Test Benches

In this appendix there is elaborated on the design and characteristics of the two test benches which are used for the equivalent force determination in section 1.2.3. The test benches have both their own 'philosophy', but share three requirements: compatibility with the F10 EAS steering gear, recreation of in-vehicle operation and the test bench has to be suitable for measuring interface states. At the start of this thesis a test bench was available, which was used in preceding projects [9, 35], to which will be referred to as **TB1**. The second test bench, **TB2** has been developed within this project in close collaboration with the 'Entwicklung Fahrdynamik' - Department at the Research and Development Centre of BMW AG in Munich, Germany.

The design of the test benches will be explained on the basis of the design of the supports and on the way the operational steering gear forces are exerted on the tie-rods.

'Rigid' Test bench

In figure F.1 three pictures are shown of test bench TB1. In figure F.3 the dynamic stiffness is shown in comparison with TB2.

Philosophy

The purpose of this test bench is to perform blocked force Transfer Path Analysis (TPA) i.e. the connection points of steering gear have to be mounted on rigid supports. To recreate true tie-rods forces, a Front Axle Carrier (FAC) with suspension and wheels are used. The FAC is modified such that the steering gear is cut loose and not connected to the FAC via its connection points.

Supports

The steering gear is mounted on four 60 mm steel cylindrical supports with triangular stability fins, which are welded to a steel slab. Between the steering gear and the supports a cone-shaped adapter is mounted (60-34 mm). Between the adapter and the support, the force

sensor is located which has an equal diameter of 60 mm. The heights of the supports are chosen such that the steering gear is in the same position with respect to the front part of the car. All four supports are equipped with a 3D force sensors and 4 3D accelerometers all round the top of each support.

Tie-rod forces

The FAC with the suspension and wheels on concrete slabs make that true steering kinematics are present on the test bench. However, the magnitude of the forces in the tie-rods are mainly due to the of weight of the vehicle, which is lacking. This is overcome by adding a dummy engine with a mass of 200 kg. The remaining lacking force on the front-train of the test bench is exerted by a bridge, which can be pneumatically adjusted in height to control the force. The bridge is equipped with load-cells to tune the force on the FAC.

Dynamics

In table F.1 the most important eigen-frequencies are shown. In figure F.3 the dynamic stiffness of the test bench is shown. In figure F.4 the most important singular values resulting from the Complex Mode Indicator Function (see appendix E) are shown.

VP1/VP2		VP3/VP4	
1047	1st bending X	540	1st bending X
1061	1st bending Y	561	1st bending Y
3162	1st rotation Z-axis	2508	1st rotation Z-axis
6314	1st Bending Z	6168	1st bending Z

Table F.1: *the most important eigen-frequencies of TB1.*

Remarks

As the front axle carrier and the steering gear are not connected and the steering gear in operation exerts a significant force (2.5 kN) on the wheel suspension, there is relative motion between the two structures. The kinematics of the wheel suspension causes an additional disadvantage by lifting and bending the FAC when steering towards the maximum angle.

'Compliant' Test Bench

In figure F.2 three pictures are shown of test bench TB2. In figure F.3 the dynamic stiffness is shown in comparison with TB1.

Philosophy

In order to improve the signal spectra for the determination of the Frequency Response Functions (FRFs) for the model based equivalent force determination schemes from section 1.2.3 and the observability of modes in every direction, it was chosen to design asymmetric and more compliant supports.

An additional benefit of a more compliant test bench, is higher signal-to-noise ratios on the accelerometers under operational conditions. Furthermore, a new design of supports ensures compatibility on advanced steering gear test facilities at the R&D of BMW AG. These test-rigs

allow communication between the PAK MKII measurement system for the operational measurements and the operational states of the test-bench, which simplifies the data processing. Furthermore, additional states of the steering gear can be evaluated more easily. **Supports**

The supports are designed with two key criteria, the observability of modes in every direction i.e. asymmetric supports and the rigid behaviour of the support close to the coupling point of the steering gear for the assumption of rigid Interface Displacement Modes (section 2.1). Furthermore, the geometry of the supports is designed for comfortable access to force impact locations and the adhesion of four 3D accelerometers in the vicinity of the virtual point. For the above reasons, the support has a massive aluminium top side on four rectangular beams. For compatibility to the steering gear test benches, the height of the centre of rack bar in the steering gear is fixed at 179 mm. This dimension constrains the height of supports to 98 mm for VP1/VP2 and 179.6 mm. A static, dynamic and fatigue analyses have been performed on the design of the supports to verify whether the design criteria have been met. This report is available for the interested reader.

Tie-rod forces

The test facility has been equipped with hydraulically controlled cylinders to actuate a piston in a linear motion. The forces produced by these actuators can be controlled with respect to e.g. rack bar position and therefore allows the reproduction of numerous force profiles.

Dynamics

As no structure in nature is fully rigid, the dynamics of the test bench TB1 are measured. In table F.2 the most important eigen-frequencies are shown. The table shows an eigen-frequency of 276 Hz. In figure F.3 the dynamic stiffness of the test bench is shown. In figure F.5 the most important singular values resulting from the Complex Mode Indicator Function (see appendix E) are shown.

VP1/VP2		VP3/VP4	
1103	1st bending X	363	1st bending X
1185	1st bending Y	509	1st bending Y
2664	1st rotation Z-axis	1251	1st rotation Z-axis
6142	1st Bending Z	3239	1st bending Z

Table F.2: *the most important eigen-frequencies of TB2.*

Remarks

The test-bench and its equipment (steering robot, force actuators) are placed on a large table which is decoupled from the world by springs (± 5 Hz). The structural noise induced by these systems is higher than expected.

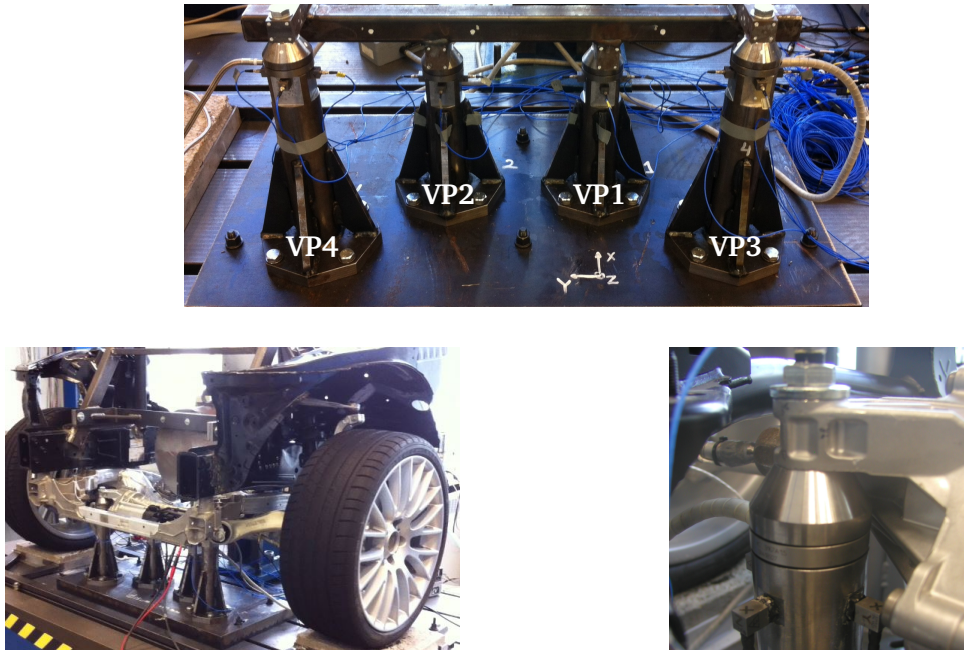


Figure F.1: An overview of the supports of TB1 and the measurement equipment (top fig.). In the bottom left figure, the front axle carrier and the dummy engine and on the right, a zoom-in on a support equipped with force- and acceleration sensors.

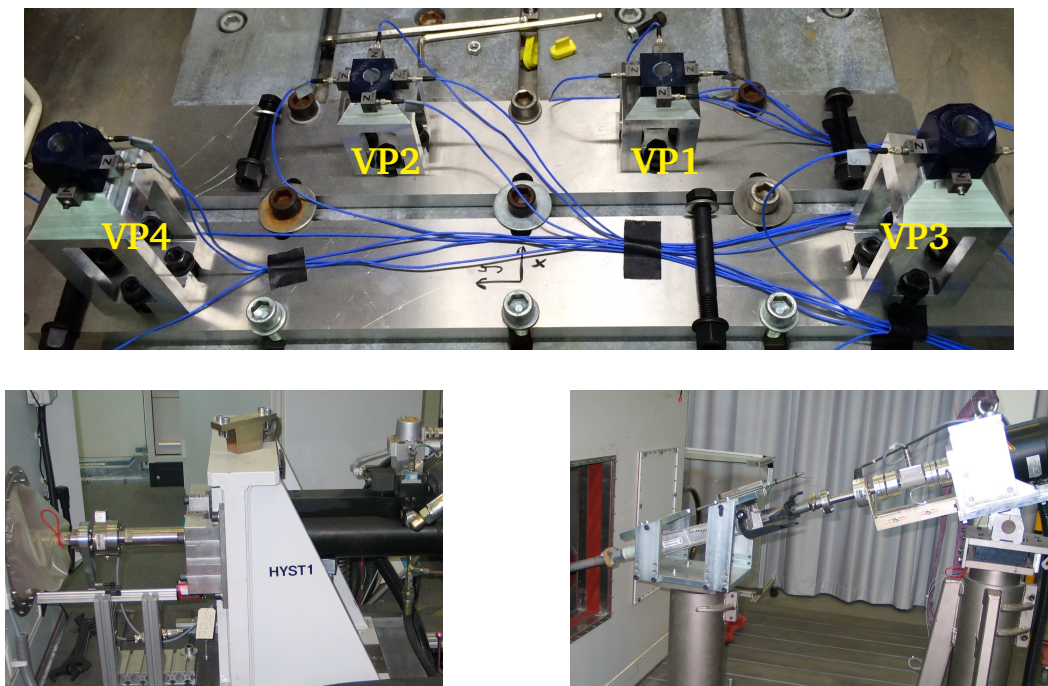


Figure F.2: An overview of the supports of TB2 and the measurement equipment (top fig.). In the bottom left figure, the hydraulic force actuator and on the right, the steering robot.

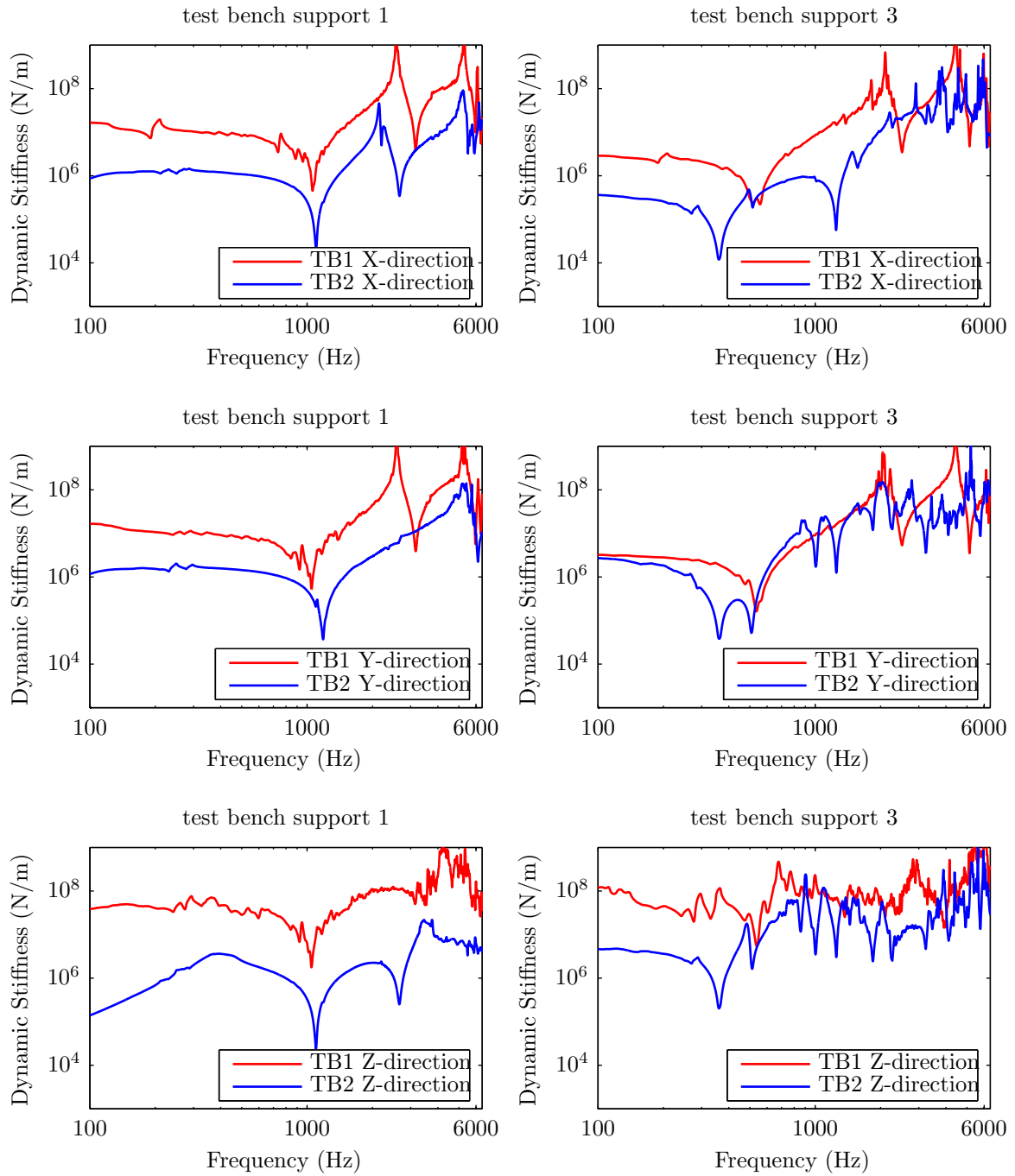


Figure F.3: The dynamic stiffness of both test benches in all 3 directions, on the left hand-side of support VP1, on the right hand-side of VP3.

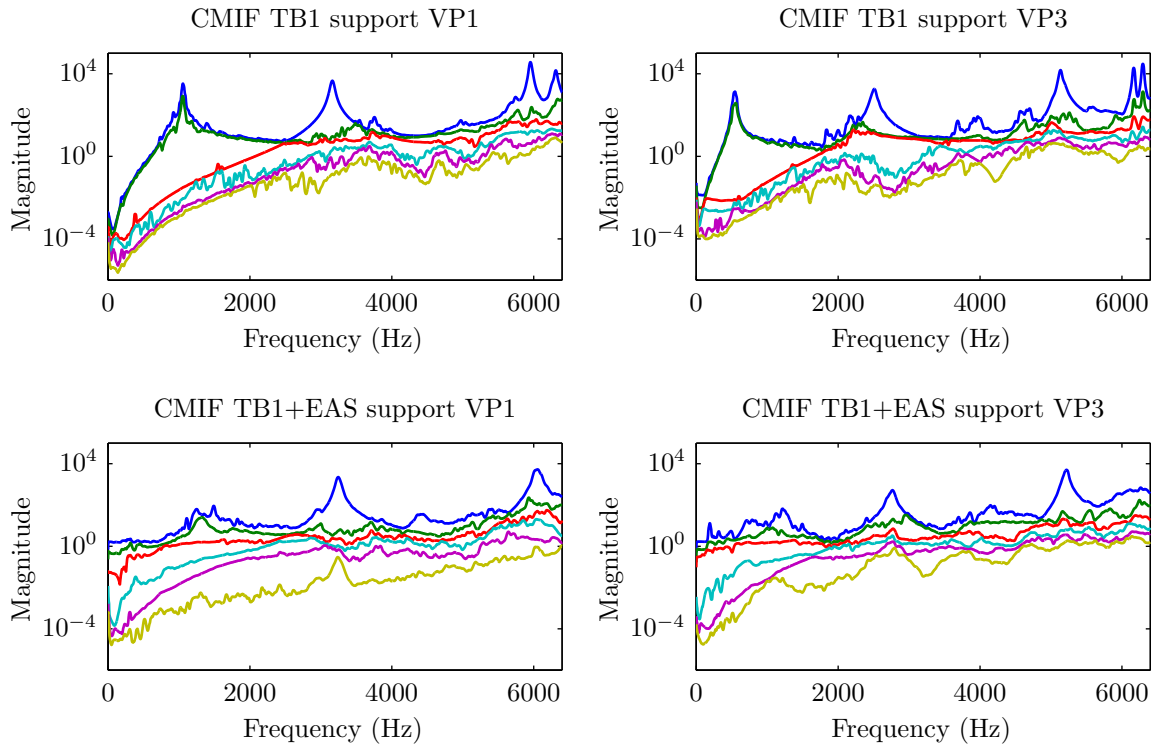


Figure F.4: The Complex Mode Indicator Function for test bench TB1 for the supports VP1 and VP3. The upper figures correspond to the test bench, the lower figures to the test bench with the steering gear.

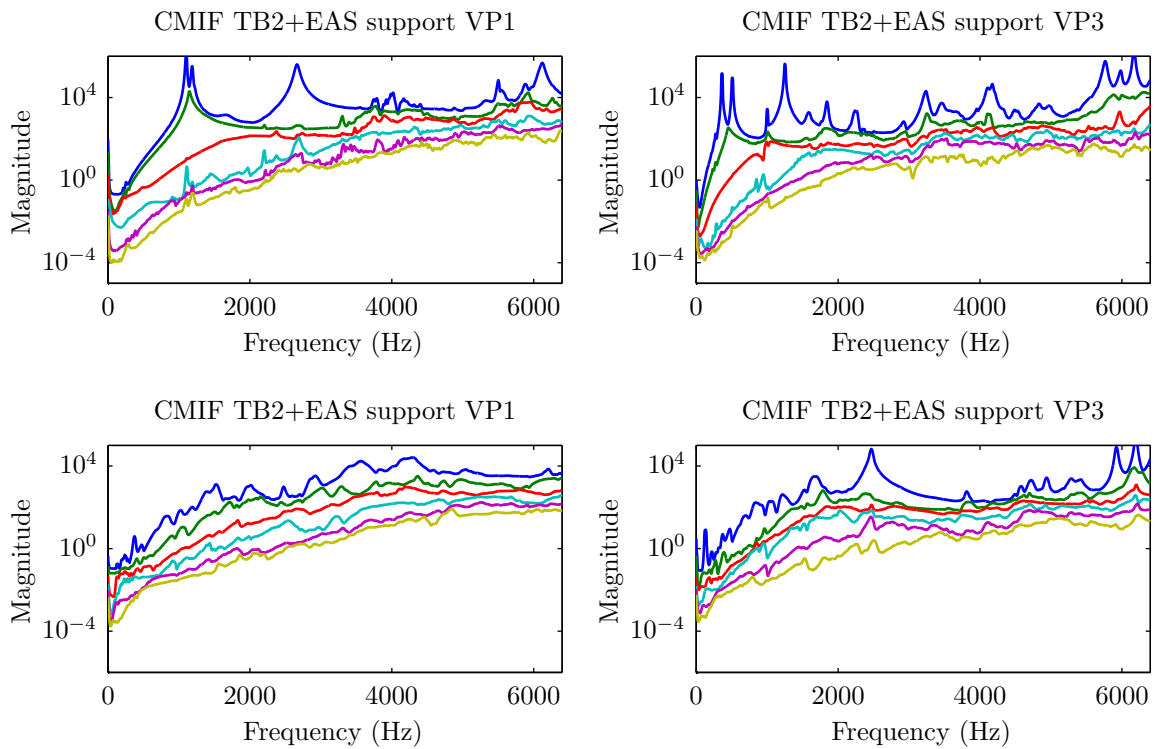


Figure F.5: The Complex Mode Indicator Function for test bench TB2 for the supports VP1 and VP3. The upper figures correspond to the test bench, the lower figures to the test bench with the steering gear.

Appendix G

Measurement Equipment

In appendix the measurement equipment is listed, the most important properties are listed.

MüllerBBM VAS PAK MKii	
software	PAK 5.7
digital sampling	24 bit
sampling rate	16384 Hz

PCB Piezotronics Triaxial ICP accelerometer (356A32)	
Sensitivity	10.2 $mV/(m/s^2)$ ($\pm 10\%$)
Measurement Range	$\pm 491 (m/s^2)$
Frequency Range ($\pm 10\%$)	0.7 – 5000 Hz
Resonance Frequency	25 kHz
Size:	11.4 × 11.4 × 11.4 mm
Weight:	5.4 gram
Mounting	Loctite 496 (glue)

PCB Piezotronics ICP Hammer (8206-003)

Sensitivity:	2.25 mV/N
Measurement Range	± 2224 N pk
Hammer tip	Medium (White plastic, Delrin)

Brüel & Kjær microphones (2669)

Sensitivity	50 mV/Pa
Frequency range	6.3 Hz - 20 kHz
Dynamic range	14.6 - 146 dB
Preamplifier	type 2669-L

Kistler 3D Force Sensor (9167A)

Sensitivity	-3.8 pC/N (x,y-dir.) -4.2 pC/N (z-dir.)
Measurement Range	-20 ... 20 kN
Threshold	$< 1 \cdot 10^{-2}$ N
Size	60 mm (diameter) \times 12 (mm)

Appendix H

Matlab Toolbox

The software package MATLAB is used to process all data in this thesis. Object Orientated Programming (OOP) provides the ability to manage large data sets in a rather structured manner. Data with similar *attributes* describe classes on which procedures are applied, also known as *methods*.

In the following list, the classes in the Dynamic Substructuring toolbox are shortly described.

ds.frfmatrix Used for editing, analysing and visualisation of Frequency Response Functions (FRFs) vectors/matrices. Properties of the channels and reference channels in other classes can be coupled to the `ds.frfmatrix` class.

ds.point superclass for the `ds.virtualpoint` and `ds.measpoint`. In these objects all properties of either a virtual point, of the measurement point i.e. (reference-) channels are specified. Properties on the type of measurement quantity and position/orientation of measurement equipment are described in this class.

ds.idm class for building a Interface Deformation Mode (IDM) and its matrices described in section 2.1. This classes uses the properties of the `ds.point` class and its subclasses.

ds.timeblocks This class is used for the collection of operational measurements and visualisation of data in the time domain. With the use of the labelling blocks of data with time intervals with the `ds.label` class data is collected.

ds.fftblocks Similar to the `ds.timeblocks` class, but the labelled time data is transformed to the frequency domain.

Bibliography

- [1] R. Allemang, W. Fladung, and A.W. Phillips. “The Complex Mode Indicator Function (CMIF) as a Parameter Estimation Method”. In: *IMAC XVI - 16th International Modal Analysis Conference*. 1998.
- [2] R.J. Allemang. “The Modal Assurance Criterion: Twenty Years of Use and Abuse”. In: *Sound and Vibration Magazine* (Aug. 2003), pp. 14–21. ISSN: 1541-0161.
- [3] M.S. Allen, R.L. Mayes, and E.J. Bergman. “Experimental modal substructuring to couple and uncouple substructures with flexible fixtures and multi-point connections”. In: *Journal of Sound & Vibration* 329.23 (2010), pp. 4891 –4906. ISSN: 0022-460X. DOI: [10.1016/j.jsv.2010.06.007](https://doi.org/10.1016/j.jsv.2010.06.007).
- [4] P. Avitabile. “101 Ways to extract modal parameters - which is the one for me?” In: *Proceedings of the XVIII International Modal Analysis Conference, Orlando, FL*. 2005.
- [5] P. Avitabile. “When I perform impact testing, the input spectrum looks distorted - do you think my FFT analyzer has a problem?” *SEM Experimental Techniques* - April 2005.
- [6] E. Balmès. “Frequency Domain Identification of Structural Dynamics Using the Pole/Residue Parametrization”. In: *Proceedings of the XIV International Modal Analysis Conference, Dearborn, MI*. 1995.
- [7] E. Barten, M.V. van der Seijs, and D. de Klerk. “A Complex Power approach to characterise Joints in Experimental Dynamic Substructuring”. In: (2013).
- [8] S. Bograd, P. Reuss, A. Schmidt, L. Gaul, and M. Mayer. “Modeling the dynamics of mechanical joints”. In: *Mechanical Systems and Signal Processing* 25.8 (2011), pp. 2801 –2826. ISSN: 0888-3270. DOI: <http://dx.doi.org/10.1016/j.ymssp.2011.01.010>.
- [9] Daniël D. van den Bosch, Maarten V. van der Seijs, and Dennis de Klerk. “Validation of Blocked-Force Transfer Path Analysis with Compensation for Test Bench Dynamics”. In: *Proceedings of the XXXII International Modal Analysis Conference, Orlando, FL*. Society for Experimental Mechanics. Bethel, CT, 2014.
- [10] R.R. Craig and A.J. Kurdila. *Fundamentals of Structural Dynamics*. New York, London, Sydney: John Wiley & Sons, Inc., 2006.

- [11] R.R.J. Craig and M.C.C. Bampton. "Coupling of Substructures Using Component Mode Synthesis". In: *AIAA Journal* 6 (1968), pp. 1313–1319.
- [12] M.L.M. Duarte and D.J. Ewins. "Some Insights into the Importance of Rotational Degrees of Freedom and Residual Terms in Coupled Structure Analysis". In: *Proceedings of the XIII International Modal Analysis Conference, Nashville, TN*. Society for Experimental Mechanics. 1995, pp. 164–170.
- [13] A. S. Elliott and A. T. Moorhouse. "Characterisation of structure borne sound sources from measurement in-situ". In: cited By (since 1996)0. 2008, pp. 1477–1482.
- [14] A. S. Elliott, A. T. Moorhouse, T. Huntley, and S. Tate. "In-situ source path contribution analysis of structure borne road noise". In: *Journal of Sound and Vibration* 332.24 (2013), pp. 6276–6295.
- [15] D.J. Ewins. *Modal Testing, Theory, Practice and Application*. New York, London, Sydney: John Wiley & Sons, Inc., 1984.
- [16] D. Findeisen. *System Dynamics and Mechanical Vibrations*. Springer, 2000.
- [17] W.A. Fladung. "The development and implementation of multiple reference impact testing". MA thesis. University of Cincinnati, 1994.
- [18] P. Gardonio and M.J. Brennan. "On the origins and development of mobility and impedance methods in structural dynamics". In: *Journal of Sound and Vibration* 249.3 (2002), pp. 557 –573. ISSN: 0022-460X. DOI: <http://dx.doi.org/10.1006/jsvi.2001.3879>.
- [19] BMW GROUP. URL: <http://www.bmwgroup.com/>.
- [20] E.L. Hixson. "Mechanical Impedance and Mobility". In: *Shock and Vibration Handbook*. Ed. by C.M. Harris and C.E. Crede. 1st. McGraw-Hill, 1961. Chap. 10, pp. 1–59.
- [21] B. Jetmundsen, R.L. Bielawa, and W. G. Flannelly. "Generalized Frequency Domain Substructure Synthesis". In: *Journal of the American Helicopter Society* 33.1 (1988), pp. 55–64. DOI: [10.4050/JAHS.33.55](https://doi.org/10.4050/JAHS.33.55).
- [22] D. de Klerk. "Dynamic Response Characterization of Complex Systems through Operational Identification and Dynamic Substructuring". PhD thesis. Delft University of Technology, 2009.
- [23] D. de Klerk and D.J. Rixen. "Component transfer path analysis method with compensation for test bench dynamics". In: *Mechanical Systems and Signal Processing* 24.6 (2010), pp. 1693 –1710. ISSN: 0888-3270. DOI: [10.1016/j.ymsp.2010.01.006](https://doi.org/10.1016/j.ymsp.2010.01.006).
- [24] D. de Klerk, D.J. Rixen, and J. de Jong. "The Frequency Based Substructuring Method reformulated according to the Dual Domain Decomposition Method". In: *Proceedings of the XXIV International Modal Analysis Conference, St. Louis, MO*. Society for Experimental Mechanics. Bethel, CT, 2006.
- [25] D. de Klerk, D.J. Rixen, and S.N. Voormeeren. "A General Framework for Dynamic Substructuring. History, review and classification of techniques". In: *AIAA Journal* 46.8 (2008), pp. 1169–1181.
- [26] D. de Klerk, D.J. Rixen, S.N. Voormeeren, and F. Pasteuning. "Solving the RDoF Problem in Experimental Dynamic Substructuring". In: *Proceedings of the XXVI International Modal Analysis Conference, Orlando, FL*. Society for Experimental Mechanics. Bethel, CT, 2008.

- [27] LMS International. *Transfer Path Analysis: The Qualification and Quantification of Vibroacoustic Transfer Paths*. Leuven, Belgium, 1995.
- [28] A. T. Moorhouse, T.A. Evans, and A. S. Elliott. “Some relationships for coupled structures and their application to measurement of structural dynamic properties in situ”. In: *Mechanical Systems and Signal Processing* 25.5 (2011), pp. 1574–1584.
- [29] A.T. Moorhouse, A.S. Elliott, and T.A. Evans. “In situ measurement of the blocked force of structure-borne sound sources”. In: *Journal of Sound & Vibration* 325.4–5 (2009), pp. 679–685. ISSN: 0022-460X. DOI: <http://dx.doi.org/10.1016/j.jsv.2009.04.035>.
- [30] Edward Lawry Norton. *Design of finite networks for uniform frequency characteristic*. Tech. rep. Technical Report TM26–0–1860, Bell Laboratories, 1926.
- [31] Juha Plunt. “Finding and fixing vehicle NVH problems with transfer path analysis”. In: *Sound and vibration* 39.11 (2005), pp. 12–17.
- [32] D. Rixen, A. Boogaard, M.V. van der Seijs, G. van Schothorst, and T. van der Poel. “Vibration source description in substructuring: a theoretical depiction”. In: *Mechanical Systems and Signal Processing* (2014). (submitted).
- [33] D.J. Rixen. “How Measurement Inaccuracies Induce Spurious Peaks in Frequency Based Substructuring”. In: *Proceedings of the XXVI International Modal Analysis Conference, Orlando, FL*. Society for Experimental Mechanics. Bethel, CT, 2008.
- [34] B. Schwarz and M. Richardson. “Scaling Mode Shapes Obtained From Operating Data”. In: *Journal of Sound and Vibration* (2003).
- [35] M. van der Seijs, E. Pasma, D. de Klerk, and D. Rixen. “A robust Transfer Path Analysis method for steering gear vibration on a test bench”. In: *26th International ISMA Noise and Vibration Engineering Conference*. 2014.
- [36] M.V. van der Seijs, D.D. van den Bosch, D.J. Rixen, and D. de Klerk. “An improved methodology for the virtual point transformation of measured frequency response functions in dynamic substructuring”. In: *COMPADYN 2013 4th, ECCOMAS Thematic Conference on Computational Methods in Structural Dynamics and Earthquake Engineering*. Ed. by M. Papadrakakis, V. Papadopoulos, and V. Plevris. Kos Island, Greece, 12 – 14 June 2013.
- [37] M.V. van der Seijs, D. de Klerk, D.J. Rixen, and S. Rahimi. “Validation of current state Frequency Based Substructuring Technology for the characterisation of Steering Gear – Vehicle Interaction”. In: *Proceedings of the XXXI International Modal Analysis Conference, Los Angeles, CA*. Society for Experimental Mechanics. Bethel, CT, 2013.
- [38] L Thévenin. “Sur un nouveau théoreme d’électricité dynamique [On a new theorem of dynamic electricity]”. In: *CR des Séances de l’Académie des Sciences* 97 (1883), pp. 159–161.
- [39] A.N. Thite and D.J. Thompson. “The quantification of structure-borne transmission paths by inverse methods. Part 1: Improved singular value rejection methods”. In: *Journal of Sound and Vibration* (2003).

- [40] S.N. Voormeeren and D.J. Rixen. “A Dual Approach to Substructure Decoupling Techniques”. English. In: *Structural Dynamics, Volume 3*. Ed. by Tom Proulx. Conference Proceedings of the Society for Experimental Mechanics Series. Springer New York, 2011, pp. 601–616. ISBN: 978-1-4419-9833-0.
- [41] S.N. Voormeeren and D.J. Rixen. “A family of substructure decoupling techniques based on a dual assembly approach”. English. In: *Mechanical Systems and Signal Processing* 27.18 (2012), p. 379.